J. Fluid Mech. (1992), *vol.* 245, *pp.* 367–400

On the instability of boundary layers on heated flat plates

By PHILIP HALL[1] AND HELEN MORRIS[2]

[1] Department of Mathematics, University of Manchester, Manchester M13 9PL, UK

[2] Department of Mathematics, University of Exeter, Exeter EX4 4QE, UK

(Received 6 August 1991)

The stability of a boundary layer on a heated flat plate is investigated in the linear regime. The flow is shown to be unstable to longitudinal vortex structures which develop in a non-parallel manner in the streamwise direction. Solutions of the non-parallel equations are obtained numerically at $O(1)$ values of the appropriate stability parameter, i.e. the Grashof number. We investigate the particular cases in which instability is induced by localized or distributed wall roughness or non-uniform wall heating. The case when the vortices are induced by free-stream disturbances is also considered. We then investigate the high-Grashof-number limit and the fastest growing mode. The fastest growing mode is found to be governed by a quasi-parallel theory and occurs at high wavenumbers. The wavenumber and growth rate of the fastest growing mode are found in closed form. At low wavenumbers the vortex instability is shown to be closely related to Tollmein–Schlichting waves; the effect of wall heating or cooling on the latter type of instability is discussed.

1. Introduction

Our concern is with the instability of forced-convection boundary layers over horizontal heated flat plates. Such flows are unstable to at least two types of hydrodynamic instabilities: first we expect a convective Rayleigh–Bénard type of instability because the fluid at the plate is hotter than the fluid in the free stream; secondly we expect a Tollmien–Schlichting type of instability because of the similarity of the flow to isothermal boundary layers where that type of disturbance is known to be important. In this paper we shall primarily be concerned with the vortex mode of instability which we investigate in a self-consistent manner using an approach suggested by related work on the closely connected Görtler vortex problem, see for example Hall (1990) and Denier, Hall & Seddougui (1991). However, in the small-wavenumber limit of the vortex mode we find an unexpected relationship between the vortex mode and Tollmien–Schlichting waves; in effect we find that in this limit the two modes coalesce. We are thus able to describe both propagating vortex modes and determine the effect of wall heating on the growth of longitudinal vortex structures in boundary layers.

Interest in forced-convection boundary layers is generated by the wide range of practical problem where such flows occur; in particular we refer to the heat transfer problems associated with solar heating, electronic devices and nuclear reactors. In such situations it is important to know the parameter regime where instability begins because of the associated change in heat transfer properties of the flow.

Experimental investigations of the vortex mode of instability in a forced-convection boundary layer have been carried out by Gilpin, Imura & Cheng (1978) for water, and by Wang (1982) for air. In this paper we shall concentrate on boundary layers in air. In fact both Wang and Gilpin *et al.* have demonstrated the existence of the onset of a vortex mode of instability and suggested that this onset occurs at the same value of $G_x Re_x^{-\frac{3}{2}}$ when the local Grashof number G_x and Reynolds number Re_x are varied. We also note that a related instability occurs in channel flows when one wall is heated; the reader is referred to the paper by Akiyama, Hwang & Cheng (1971) for an experimental investigation of that problem.

Theoretical investigations of the vortex mode of instability have been given by Wu & Cheng (1976) and Moutsoglou, Chen & Cheng (1984). In both of these calculations, and all other investigations we are aware of, the growth of the boundary layer is not taken into account in a self-consistent manner. In effect it has been previously assumed that the streamwise variation of the vortex mode is on a short lengthscale compared to that over which the basic flow evolves. However, at finite values of the Grashof number, where instability first sets in, the destabilizing buoyancy forces are sufficient only to provoke a response on the same streamwise lengthscale as that over which the basic state develops. In that case it follows that previous calculations have ignored a crucial property of the vortex instability; thus the intrinsic non-parallel nature of the disturbance has been neglected.

A similar parallel-flow assumption was made for many years by researchers concerned with the Görtler mechanism in curved boundary layers. More recently Hall (1983) showed that the non-parallel nature of the vortex mode at finite values of the Görtler number must be accounted for by numerical investigations of the disturbance equations. At high Görtler numbers analytical progress can be made because the growth rates become large and non-parallel effects may be neglected at zeroth order; see Hall (1982*a*, *b*), Denier *et al.* (1991).

In this paper we shall concentrate on the vortex mode at finite values of the appropriate stability parameter, i.e. the Grashof number. A question of fundamental importance in this, and in fact any other parameter regime, is that of what is the physical process which triggers disturbances in the flow and causes them to amplify. This, the so-called receptivity problem, has been addressed for the Görtler problem by Hall (1990), and Denier *et al.* (1991). In particular the receptivity problems for wall roughness and free-stream disturbances were investigated in those papers. The corresponding receptivity problems will be investigated here for heated boundary layers.

Thus, following a formulation of the instability equations in §2, we shall in §3 investigate the stability problem at finite Grashof numbers using a numerical scheme outlined there. In §4 we concentrate on the amplification of vortex disturbances induced by localized wall roughness or non-uniform wall heating. In §5 we will investigate the generation of vortex disturbances by free-stream inhomogeneities, whilst in §6 some results for distributed forcing are given.

In §7 we concentrate on the high-Grashof-number limit; this regime is relevant to disturbances which have passed through the order-one Grashof-number regime without sufficient amplification to be controlled by nonlinear effects. At order-one wavenumbers we show that the now unique growth rate is determined by an inviscid eigenvalue problem. However, the growth rate predicted by the inviscid theory increases monotonically with the wavenumber so that the fastest growing mode cannot be described by a purely inviscid theory. The fastest growing mode is found to have a high wavenumber and to be governed by a quasi-parallel theory. At small

vortex wavenumbers viscous effects again dominate and we show that the vortex mode ultimately takes on a triple-deck-like structure. This structure is shown to describe both vortex and Tollmien–Schlichting modes. Finally in §8 we compare our results with previous experimental and theoretical work and draw some conclusions.

2. Formulation of the instability equations

We consider the flow of a viscous fluid over a heated semi-infinite flat plate. Suppose that U_∞ is a typical free-stream velocity, L is a typical lengthscale in the streamwise direction and ν is the kinematic viscosity. The Reynolds number is defined by $Re = U_\infty L/\nu$ and throughout we assume that $Re \gg 1$. The wall is defined with respect to dimensional Cartesian coordinates x^*, y^*, z^* by

$$y^* = L\Delta\, Re^{-\frac{1}{3}} f(x^*/L, Re^{\frac{1}{3}} z^*/L),$$

where Δ is a small dimensionless constant. We take the temperature of the fluid a long way from the plate to be zero whilst at the plate it is given by

$$T^* = T_0 + (T_0 - T_\infty)\,\Delta g(x^*/L, Re^{\frac{1}{3}} z^*/L).$$

Here T_0 is a constant reference temperature, T_∞ is the temperature in the far-field region and g represents the effect of a slight non-uniform heating of the plate.

We define the Grashof number as

$$G_1 = L^3 \bar{g}(T_0 - T_\infty)\,\bar{\beta}\nu^{-2}$$

and we define a relation G between the Grashof number and the Reynolds number by

$$G = G_1 Re^{-\frac{8}{3}},$$

where $\bar{g}$ is the acceleration due to gravity and $\bar{\beta}$ is the coefficient of expansion. We define (x, y, z) by

$$(x, y, z) = (x^*/L, Re^{\frac{1}{3}} y^*/L, Re^{\frac{1}{3}} z^*/L)$$

and a dimensionless velocity vector by writing

$$(u^+, v^+, w^+) = (u^*, Re^{\frac{1}{3}} v^*, Re^{\frac{1}{3}} w^*)/U_\infty. \tag{2.1a}$$

We take the corresponding pressure function to be

$$p^+ = \bar{p}(x) + Re^{-\frac{1}{3}} G\bar{p}_0 + Re^{-1}(G\bar{p}_1 + \bar{p}_2 + \Delta\tilde{p}(x, y, z) + O(\Delta^2)) = p^*/(U_\infty^2 \rho), \tag{2.1b}$$

where ρ is the fluid density, p^* is the dimensional fluid pressure, and for flow past a flat plate we have $\bar{p} = 1$ and $\bar{p}_0 = 0$. We now write

$$(u^+, v^+, w^+) = (\bar{u}, \bar{v}, 0) + \Delta(\tilde{u}, \tilde{v}, \tilde{w}) + O(\Delta^2), \tag{2.1c}$$

and the temperature field then expands as

$$(T^* - T_\infty)/(T_0 - T_\infty) = T^+ = \bar{T}(x, y) + \Delta\tilde{\theta}(x, y, z) + O(\Delta^2). \tag{2.1d}$$

In the forced problem for the order-Δ field the basic velocity and temperature fields $\bar{u}, \bar{v}, \bar{T}$ will be known functions of x and y with the basic temperature field $\bar{T}$ determined by the choice of the basic flow field and boundary conditions on the temperature. The perturbed velocity and temperature fields $\tilde{u}, \tilde{v}, \tilde{w}, \tilde{\theta}$ depend on all

three dimensionless coordinates. The steady Navier–Stokes equations for the problem involving buoyancy forces are

$$u^*_{x^*}+v^*_{y^*}+w^*_{z^*}=0, \tag{2.2a}$$

$$u^*u^*_{x^*}+v^*u^*_{y^*}+w^*u^*_{z^*}=-\frac{1}{\rho}\frac{\partial p^*}{\partial x^*}+\nu(u^*_{x^*x^*}+u^*_{y^*y^*}+u^*_{z^*z^*}), \tag{2.2b}$$

$$u^*v^*_{x^*}+v^*v^*_{y^*}+w^*v^*_{z^*}=-\frac{1}{\rho}\frac{\partial p^*}{\partial y^*}+\bar{g}\bar{\beta}(T^*-T_\infty)+\nu(v^*_{x^*x^*}+v^*_{y^*y^*}+v^*_{z^*z^*}), \tag{2.2c}$$

$$u^*w^*_{x^*}+v^*w^*_{y^*}+w^*w^*_{z^*}=-\frac{1}{\rho}\frac{\partial p^*}{\partial z^*}+\nu(w^*_{x^*x^*}+w^*_{y^*y^*}+w^*_{z^*z^*}), \tag{2.2d}$$

where all quantities in the buoyancy term, except the density, are taken to be constant using a Boussinesq approximation. The energy equation takes the form

$$u^*T^*_{x^*}+v^*T^*_{y^*}+w^*T^*_{z^*}=\frac{K}{\rho C_p}(T^*_{x^*x^*}+T^*_{y^*y^*}+T^*_{z^*z^*}), \tag{2.2e}$$

where K is the thermal conductivity and C_p is the constant specific heat. It is to be noted that, since we are considering a low-speed subsonic flow, the term representing the net rate at which shearing forces perform work on the fluid is negligible.

We now write (2.2*a–d*) in dimensionless form and consider the limiting form of these equations when Δ is small and the Reynolds number is large.

At leading order $O(Re^{-\frac{1}{2}}\Delta^0)$ we obtain

$$\bar{u}_x+\bar{v}_y=0, \quad \bar{u}\bar{u}_x+\bar{v}\bar{u}_y=-\bar{p}_x+\bar{u}_{yy}, \tag{2.3a, b}$$

$$-\bar{p}_{1_y}+\bar{T}=0, \quad \bar{u}\bar{v}_x+\bar{v}\bar{v}_y=-\bar{p}_{2_y}, \quad \bar{u}\bar{T}_x+\bar{v}\bar{T}_y=(1/Pr)\,\bar{T}_{yy}, \tag{2.3c–e}$$

for the basic velocity and temperature fields, where Pr is the Prandtl number defined by $Pr=\nu\rho C_p/K$. At next order we obtain

$$\tilde{u}_x+\tilde{v}_y+\tilde{w}_z=0, \tag{2.4a}$$

$$\bar{u}\tilde{u}_x+\tilde{u}\bar{u}_x+\bar{v}\tilde{u}_y+\tilde{v}\bar{u}_y=\tilde{u}_{yy}+\tilde{u}_{zz}, \tag{2.4b}$$

$$\bar{u}\tilde{v}_x+\tilde{u}\bar{v}_x+\bar{v}\tilde{v}_y+\tilde{v}\bar{v}_y=-\tilde{p}_y+\tilde{v}_{yy}+\tilde{v}_{zz}+G\tilde{\theta}, \tag{2.4c}$$

$$\bar{u}\tilde{w}_x+\bar{v}\tilde{w}_y=-\tilde{p}_z+\tilde{w}_{yy}+\tilde{w}_{zz}, \tag{2.4d}$$

$$\bar{u}\tilde{\theta}_x+\bar{v}\tilde{\theta}_y+\tilde{u}\bar{T}_x+\tilde{v}\bar{T}_y=(1/Pr)(\tilde{\theta}_{yy}+\tilde{\theta}_{zz}). \tag{2.4e}$$

The basic flow is taken to be the Blasius velocity profile

$$\bar{u}=\bar{f}'(\eta), \bar{v}=\frac{1}{(2x)^{\frac{1}{2}}}(\eta\bar{f}'-\bar{f}),$$

where $$\bar{f}'''+\bar{f}\bar{f}''=0 \quad \text{with} \quad \bar{f}(0)=\bar{f}'(0)=0, \quad \bar{f}'(\infty)=1.$$

Then $\bar{T}$ is given by the solution of

$$\bar{T}''+\bar{f}Pr\,\bar{T}'=0, \quad \text{where} \quad \bar{T}(0)=1 \quad \text{and} \quad \bar{T}(\infty)=0.$$

Here the similarity variable η is defined by

$$\eta=y/(2x)^{\frac{1}{2}}.$$

The basic pressure $\bar{p}$ is then zero and the basic temperature profile is then a function

of just η. The boundary conditions on the order-Δ field are obtained by setting up Taylor series expansions about $y = 0$; we obtain

$$\tilde{u} = -f\bar{u}_y, \quad \tilde{v} = \tilde{w} = 0, \quad \tilde{\theta} = g - f\bar{T}_y, \quad y = 0, \qquad \tilde{u}, \tilde{v}, \tilde{w}, \tilde{\theta} \to 0, \quad y \to \infty, \tag{2.5a}$$

$$\bar{u} = \bar{v} = 0, \quad \bar{T} = 1, \quad y = 0, \qquad \bar{u} \to 1, \quad \bar{T} \to 0, \quad y \to \infty. \tag{2.5b}$$

We assume that f, g are such that we can write $f\bar{u}_y = -\tilde{F}_1(x)\,\tilde{q}(z)$, $g - f\bar{T}_y = \tilde{F}_2(x)\,\tilde{Q}(z)$ in (2.5) which enables us to Fourier transform the disturbance equations in the z-variable. Thus if we Fourier transform (2.4), (2.5) with a as the transform variable, and denote the transform of $\tilde{q}, \tilde{u}$, etc. by q, u etc. we obtain

$$u_x + v_y + iaw = 0, \tag{2.6a}$$

$$\bar{u}u_x + \bar{v}u_y + v\bar{u}_y + u\bar{u}_x = u_{yy} - a^2 u, \tag{2.6b}$$

$$\bar{u}v_x + \bar{v}v_y + v\bar{v}_y + u\bar{v}_x = -p_y + v_{yy} - a^2 v + G\theta, \tag{2.6c}$$

$$\bar{u}w_x + \bar{v}w_y = -iap + w_{yy} - a^2 w, \tag{2.6d}$$

$$u\bar{T}_x + \bar{u}\theta_x + v\bar{T}_y + \bar{v}\theta_y = \frac{1}{Pr}(\theta_{yy} - a^2\theta), \tag{2.6e}$$

$$u = qF_1, \quad v = 0, \quad w = 0, \quad \theta = QF_2, \quad y = 0, \quad u, v, w, \theta \to 0 \quad \text{as} \quad y \to \infty. \tag{2.6f}$$

We now eliminate the pressure p and the spanwise velocity component w from the above equations to give

$$(\bar{u}_{xyy} + a^4 + a^2\bar{v}_y)\,v + \bar{v}_x u_{yy} + (\bar{u}_{xxy} + a^2\bar{v}_x)\,u + \left(\bar{u}_{yy} - \bar{u}\frac{\partial^2}{\partial y^2} + a^2\bar{u}\right)v_x$$

$$+ 2\left(\bar{u}_{xy} + \bar{u}_x\frac{\partial}{\partial y}\right)u_x + v_{yyyy} - \bar{v}v_{yyy} - (\bar{v}_y + 2a^2)\,v_{yy} + (\bar{u}_{xy} + a^2\bar{v})\,v_y - a^2 G\theta = 0. \tag{2.7}$$

Hence, given the basic velocity and temperature profiles, then by solving the system of equations (2.6*b*), (2.6*e*), (2.7) subject to the boundary conditions (2.6*f*) we can determine the solution of the forced-convection problem by numerical integration for finite values of the Grashof number. In the following section we shall describe a numerical scheme which we have used to integrate the disturbance equations found above.

3. The numerical scheme and some preliminary results

The disturbance equations (2.6*b*), (2.6*e*), (2.7) are parabolic in x and hence, having imposed an initial disturbance on the flow, we can march the equations downstream from the position where the forcing begins and monitor the vortex growth or decay. The partial differential equations describing the perturbed velocity and temperature fields were integrated using a spectral collocation method with Chebychev polynomials used to approximate the normal dependence of the disturbance. The Chebychev polynomials are defined on $\alpha \in [-1, 1]$ by

$$T_k(\alpha) = \cos(k\cos^{-1}\alpha) \quad \text{for} \quad k = 0, 1, 2, \ldots,$$

and we approximate the streamwise velocity component u, for example, using an nth degree Chebychev polynomial

$$u(\alpha) = \sum_{k=0}^{n} \frac{\beta_k}{\gamma_k} T_k(\alpha), \quad \gamma_0 = 2, \quad \gamma_k = 1, \quad k = 1, 2, \ldots,$$

and β_k are the unknown Chebychev coefficients of the expansion. The change of variable (x, y) to (x, η), where $\eta = y/(2x)^{\frac{1}{2}}$, is made in the disturbance equations which are then solved on $\eta \in [0, \eta_\infty]$. The $n+1$ collocation points were chosen to be

$$\alpha_i = \cos((i-1)\pi/n), \quad 1 \leqslant i \leqslant n+1.$$

We denote the value of u at $\eta = \eta_i$, $x_j = \bar{x} + j\bar{\epsilon}$ by u_i^j, where $\eta_i = \frac{1}{2}\eta_\infty(\alpha_i + 1)$, $\bar{x}$ is the position at which the initial disturbance is imposed, j is an integer value and $\bar{\epsilon}$ is the steplength in the x-direction. A similar notation was employed for the other flow quantities. We suppose these quantities are known at the jth step and illustrate how they are advanced to $x = x_{j+1} = \bar{x} + (j+1)\bar{\epsilon}$. Consider the x-momentum equation (2.6*b*):

$$\frac{\partial^2}{\partial\eta^2} u_i^{j+1} + (\eta_i \bar{u}_i^j - \bar{v}_i^j (2x_j)^{\frac{1}{2}}) \frac{\partial}{\partial\eta} u_i^{j+1} + \left(\eta_i \frac{\partial}{\partial\eta} \bar{u}_i^j - \frac{2x_j \bar{u}_i^j}{\bar{\epsilon}} - a^2 2x_j\right) u_i^{j+1}$$

$$= v_i^j (2x_j)^{\frac{1}{2}} \frac{\partial}{\partial\eta} \bar{u}_i^j - \bar{u}_i^j \frac{2x_j u_i^j}{\bar{\epsilon}}, \quad (3.1)$$

where u_x has been replaced by its finite-difference approximation

$$u_x = (u_i^{j+1} - u_i^j)/\bar{\epsilon}.$$

We approximate u_i^{j+1} by

$$u_i^{j+1} = \sum_{k=0}^{\eta} \frac{\beta_k}{\gamma_k} T_k(\alpha),$$

and

$$\frac{\partial^l}{\partial\eta^l} u_i^{j+1} = (\tfrac{1}{2}\eta_\infty)^l \sum_{k=0}^{\eta} \frac{\beta_k}{\gamma_k} T_k^l(\alpha), \quad l = 1, 2, \ldots.$$

We are able to generate the successive Chebychev polynomials using the relationship

$$T_{k+1}(z) = 2zT_k(z) - T_{k-1}(z) \quad \text{for} \quad k > 0.$$

In a similar manner we can determine a relationship for the derivatives of the Chebychev polynomials. We rewrite (3.1) in the form

$$\frac{\beta_k}{\gamma_k}\left\{(\tfrac{1}{2}\eta_\infty)^2 T_k''(\alpha_i) + (\tfrac{1}{2}\eta_\infty)[\eta_i \bar{u}_i^j - \bar{v}_i^j (2x_j)^{\frac{1}{2}}] T_k'(\alpha_i)\right.$$

$$\left. + \left(\eta_i \frac{\partial}{\partial\eta} \bar{u}_i^j - \frac{2x_j \bar{u}_i^j}{\bar{\epsilon}} - a^2 2x_j\right) T_k(\alpha_i)\right\} = v_i^j (2x_j)^{\frac{1}{2}} \frac{\partial}{\partial\eta} \bar{u}_i^j - \bar{u}_i^j \frac{2x_j}{\bar{\epsilon}} u_i^j, \quad (3.2)$$

for $1 \leqslant k \leqslant n-1$ with $i = 1, n+1$ for each value of k.

We use the streamwise velocity boundary conditions (2.6*f*) to replace the $k = 0$, $k = n$ values in (3.2). The right-hand side of (3.2) is known and by inverting the square full matrix on the left-hand side using a Gauss–Jordan elimination method, the values of the Chebychev coefficients β_k for $0 \leqslant k \leqslant n$ can be determined. In a similar manner we can update (2.7) and (2.6*e*). The method is totally implicit so that we expect to have a numerically stable scheme for a streamwise steplength comparable with the vertical steplength. Note that the use of a spectral method leads to high resolution near the boundaries of the flow, making this method particularly suitable for the solution of boundary-layer problems. We expect faster than algebraic decay of the error term, a property generally associated with the use of a spectral method. The spanwise velocity component w can then be calculated from the

continuity equation. The parameter η_∞ was caried and $\eta_\infty = 10$ was found to provide sufficiently accurate results. The number of collocation points n is the η-direction was chosen to be 120 and the Prandtl number Pr was chosen to be 0.72, the value for air. The calculations were carried out on an AMT DAP510 and the code was written to take advantage of the architecture of that machine.

In order to validate our scheme we carried out some calculations for the case when the initial form of the disturbance is imposed and not provided by a receptivity calculation. In that case the boundary conditions at the plate and far from the wall are

$$u = v = \partial v/\partial y = \theta = 0, \quad y = 0, \tag{3.3a}$$

$$u = v = \partial v/\partial y = \theta = 0, \quad y = \infty. \tag{3.3b}$$

We also require

$$u = u_B(y), \quad v = v_B(y), \quad \theta = \theta_B(y), \quad x = \bar{x}, \tag{3.4}$$

where the initial conditions (3.4) describe some given vortex perturbation imposed on the flow at $x = \bar{x}$. This initial disturbance must be consistent with (3.3). Further constraints on the initial perturbation (3.4) are required in order to avoid singularities in the velocity and temperature fields at $x = \bar{x}$, $y = 0$. If we expand u, v, θ as Taylor series about $x = \bar{x}$ and $y = 0$ we find that the required conditions are

$$u_B''(0) = 0, \quad u_B'''(0) = a^2 u_B'(0), \tag{3.5a}$$

$$v_B^{\mathrm{iv}}(0) = 2a^2 v_B''(0), \tag{3.5b}$$

$$\theta_B''(0) = 0, \quad \theta_B'''(0) = a^2 \theta_B'(0). \tag{3.5c}$$

The perturbation imposed on the flow was taken to be either

$$u_B = \eta^6 \mathrm{e}^{-\eta^2}, \quad v_B = 0, \quad \theta_B = 0, \quad x = \bar{x}, \tag{3.6}$$

or

$$u_B = 0, \quad v_B = 0, \quad \theta_B = \eta^6 \mathrm{e}^{-\eta^2}, \quad x = \bar{x}, \tag{3.7}$$

where $\eta = y/(2x)^{\frac{1}{2}}$. Note that both (3.6) and (3.7) satisfy the conditions (3.3), (3.5). The numerical scheme described in this section was used to solve the linear disturbance equations (2.6*b*), (2.6*e*), (2.7), subject to the boundary conditions (3.3) with initial conditions given by either (3.6) or (3.7).

For the calculations reported here we took $\bar{\epsilon} = 0.1$. Of course the accuracy of our calculations was checked by varying $\bar{\epsilon}$ and the vertical grid spacing in some cases. The vortex growth downstream is determined by monitoring

$$E_1 = \int_0^\infty |\theta| \, \mathrm{d}y$$

and the local growth rate $\sigma_1(x) = (1/E_1)(\partial E_1/\partial x)$. The neutral point was taken to be the downstream location where this growth rate vanishes; the local Grashof number and wavenumber corresponding to this point are then obtained from

$$a_x = a x^{\frac{1}{2}}, \quad G_x = G x^{\frac{3}{2}}.$$

A series of neutral points were obtained for fixed $\bar{x}$ by solving the system of equations numerically for several values of the wavenumber a.

Different neutral curves were generated for fixed $G = 0.025$ by varying the location $\bar{x}$ of the initial disturbance. Figure 1 (*a–d*) demonstrates the downstream velocity and temperature fields for an initial disturbance given by (3.4) with $G = 0.025$ and $a = 0.069$. The corresponding neutral curves are given in figure 2. For an

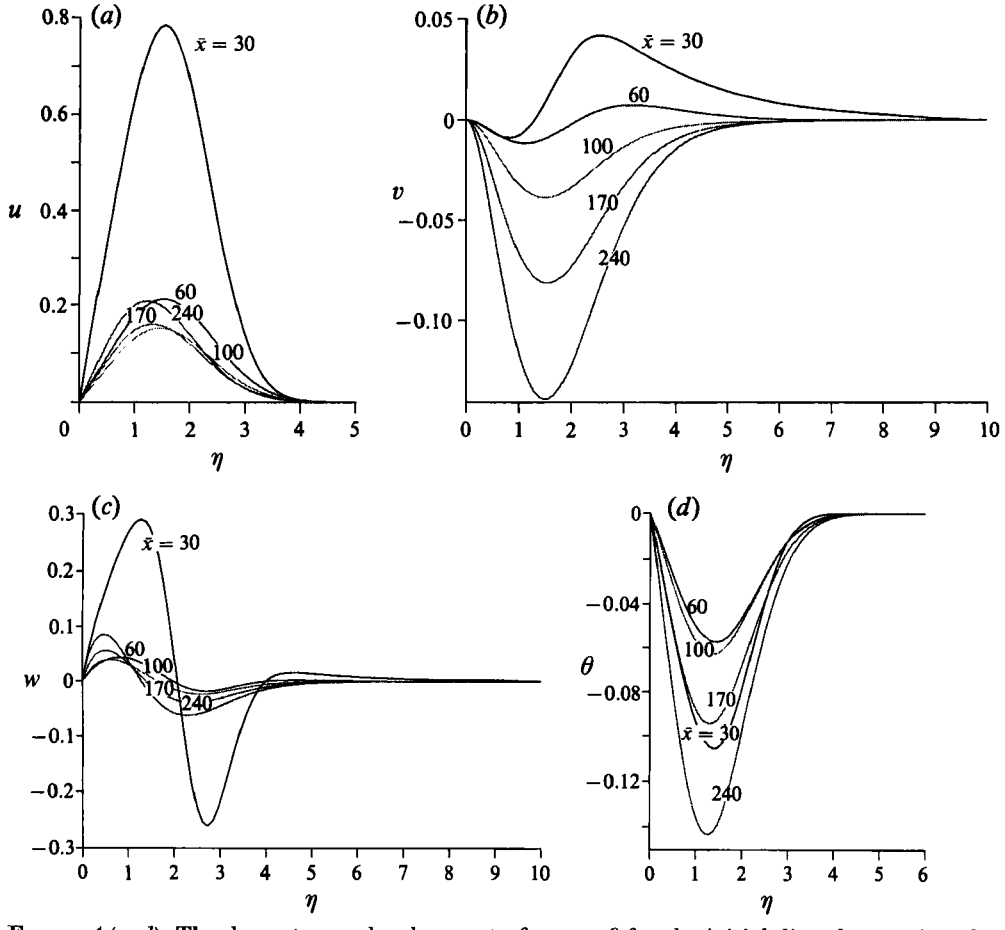

FIGURE 1 (*a–d*). The downstream development of u, v, w, θ for the initial disturbance given by (3.4) with $G = 0.025, a = 0.069$.

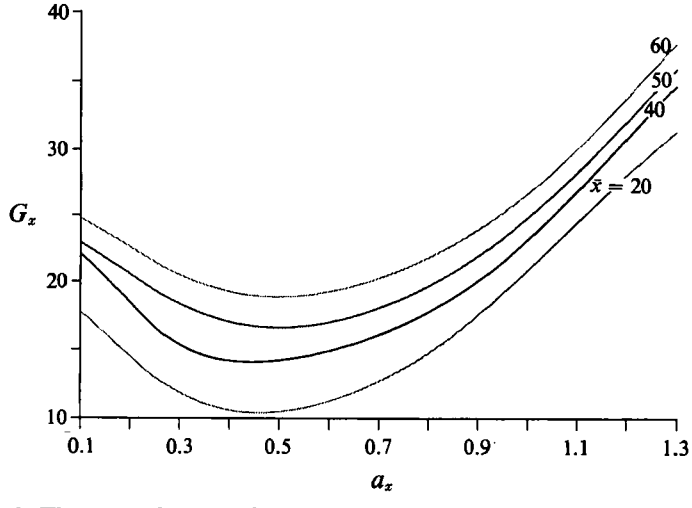

FIGURE 2. The neutral curves for different values of $\bar{x}$ for the initial conditions (3.4).

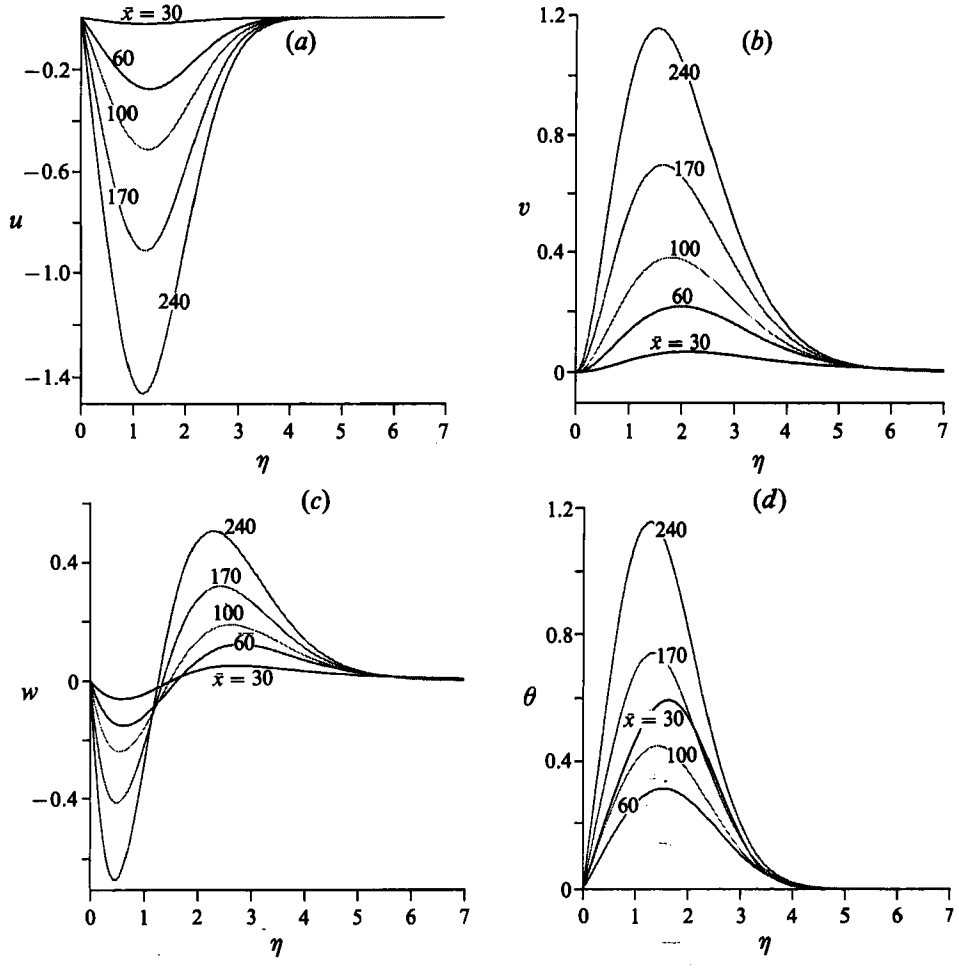

FIGURE 3(*a–d*). The downstream development of u, v, w, θ for the initial disturbance given by (3.7) with $G = 0.025, a = 0.069$.

initial disturbance of the form (3.7), the development of the velocity and temperature fields is shown in figure 3 with the corresponding neutral curves shown in figure 4. The perturbed velocity profiles for the initial disturbance given by (3.4) shown in figure 1 take the same form as those found by Hall (1983). The essential shape of the perturbed velocity and temperature components do not alter radically with increasing x. Initially the spanwise velocity component w is proportional to $\partial u/\partial x$ from continuity, since the normal velocity component v of the initial disturbance is zero. Hence both the streamwise velocity component u and w initially decay downstream of $\bar{x}$ before growing at larger values of x. The velocity and temperature profiles for a perturbation described by (3.7) are of a similar form but take the opposite sign. It is clear from figures 2 and 4 that the concept of a unique neutral curve is untenable and that the growth or decay of the resulting vortex structure is dependent upon its initial form and location. However far downstream the flow is disturbed, the growth rate $\sigma_1(x)$ is initially negative. On the right-hand branch of the neutral curve $G_x \sim a_x^4$, but for a fixed wavenumber disturbance, $G_x \sim a_x^3$ as the flow develops $G_x/a_x^4 \to 0$ and the flow is locally stable. Thus any disturbance of fixed wavelength will ultimately be stable sufficiently far downstream of the leading edge.

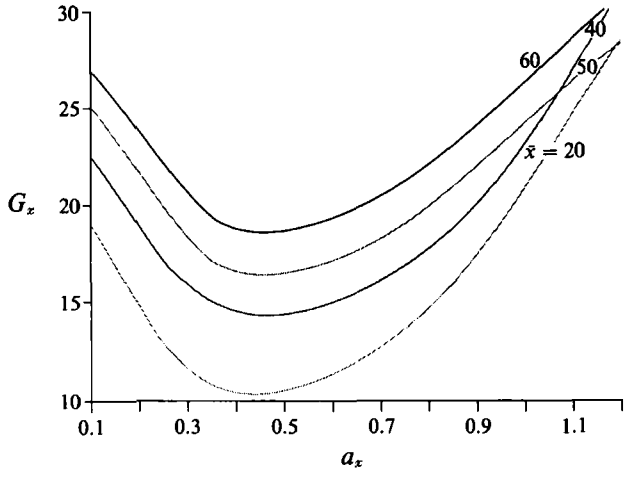

FIGURE 4. The neutral curves for different values of $\bar{x}$ for the initial conditions (3.7).

4. The localized forcing problem

We now consider the case when the wall forcing is described by isolated forcing functions and therefore allow $F_1(x), F_2(x)$ to vary on a relatively fast $O(\epsilon)$ lengthscale. We write

$$X = (x-\bar{x})/\epsilon, \tag{4.1}$$

where ϵ is small and we assume that the forcing starts at $x = \bar{x}$. By employing a faster streamwise lengthscale for the isolated heating function problem we will provide unique initial conditions for the disturbance equations. We take $F_{1,2}(x) = F^+_{1,2}(X)$ and choose $\bar{x} = \frac{1}{2}$ without loss of generality. This fixes the original lengthscale L in terms of the distance between the leading edge and the starting point of the forcing. In the following discussion we have also taken $q = Q = 1$; the more general case can be recovered by inserting these factors in our final results. In order to find the forced flow in a neighbourhood of $\bar{x}$ we note that $\bar{u}u_x \sim u_{yy}$ for small y if $y \sim O(\epsilon^{\frac{1}{3}})$ and hence the convection and diffusion effects are of the same order of magnitude in a layer of depth $\epsilon^{\frac{1}{3}}$. For small y the basic velocity and temperature fields can be approximated by

$$(\bar{u}, \bar{v}, \bar{T}) = (\lambda y, \mu y^2, 1+\phi y)+\ldots,$$

where $\lambda = \overline{u_y}(\frac{1}{2}, 0)$, $\mu = \overline{v_{yy}}(\frac{1}{2}, 0)$, $\phi = \overline{T_y}(\frac{1}{2}, 0)$ and the wall forcing implies that u, θ are $O(1)$ in the region $y \sim O(\epsilon^{\frac{1}{3}})$. We define $\xi = y/\epsilon^{\frac{1}{3}}$ and assume that $\xi = O(1)$. The appropriate expansions near the wall are then found to be

$$(u, v, w, p, \theta) = (u_0(X,\xi)+\ldots, \epsilon^{\frac{2}{3}}v_0(X,\xi)+\ldots, \epsilon^{-1}w_0(X,\xi) + \ldots, \epsilon^{\frac{5}{3}}p_0(X,\xi)+\ldots, \theta_0(X,\xi)+\ldots). \tag{4.2}$$

The expansions (4.2) are substituted into (2.7), and comparing leading-order terms yields

$$\left\{\frac{\partial^2}{\partial\xi^2} - \lambda\xi\frac{\partial}{\partial X}\right\}\frac{\partial^2 v_0}{\partial\xi^2} = 0. \tag{4.3}$$

If we now take the Laplace transform of (4.3) with s as the Laplace transform variable we can show that

$$\frac{\mathrm{d}^2\tilde{v}_0}{\mathrm{d}\xi^2} = A\,\mathrm{Ai}\,(\lambda^{\frac{1}{3}}s^{\frac{1}{3}}\xi), \qquad \frac{\mathrm{d}\tilde{v}_0}{\mathrm{d}\xi} = A\int_0^\xi \mathrm{Ai}\,(\lambda^{\frac{1}{3}}s^{\frac{1}{3}}\xi)\,\mathrm{d}\xi + B, \tag{4.4}$$

where $\tilde{\tilde{v}}_0(s,\xi)$ is the Laplace transform of $v_0(X,\xi)$, Ai is the Airy function and A and B are constants. Transforming the continuity equation and evaluating it at the wall yields

$$B = -\tilde{\tilde{F}}_1(s),$$

where $\tilde{\tilde{F}}_1(s)$ is the Laplace transform of $F_1^+(X)$. Furthermore we require that $\tilde{\tilde{v}}_{0\xi}$ vanishes at infinity, so that

$$A = -3B\lambda^{\frac{1}{3}}s^{\frac{1}{3}},$$

and

$$\tilde{\tilde{v}}_0 = -s\tilde{\tilde{F}}(s)\left\{\xi - 3\int_0^{\xi} d\xi\left(\int_0^{(\lambda s)^{\frac{1}{3}}\xi} \mathrm{Ai}\,(y)\,dy\right)\right\}. \tag{4.5}$$

The transformed temperature perturbation and streamwise velocity component are obtained from (2.6*b*, *e*) which give

$$(d^2/d\xi^2 - \lambda\xi s)\,\tilde{\tilde{u}}_0 = \tilde{\tilde{v}}_0\,\lambda, \tag{4.6}$$

$$((1/Pr)\,d^2/d\xi^2 - \lambda\xi s)\,\theta_0 = \tilde{\tilde{v}}_0\,\lambda, \tag{4.7}$$

where θ_0 is the transformed zeroth-order temperature field. For large ξ the asymptotic forms of $\tilde{\tilde{u}}_0$, $\tilde{\tilde{v}}_0$ and θ_0 are given by

$$\tilde{\tilde{u}}_0 \sim -3\tilde{\tilde{F}}_1 s^{-\frac{1}{3}}\lambda^{-\frac{1}{3}}\omega\xi^{-1} + \ldots = -3\tilde{\tilde{F}}_1 s^{-\frac{1}{3}}\lambda^{-\frac{1}{3}}\omega\epsilon^{\frac{1}{3}}y^{-1} + \ldots, \tag{4.8a}$$

$$\tilde{\tilde{v}}_0 \sim 3\tilde{\tilde{F}}_1 s^{\frac{2}{3}}\lambda^{-\frac{1}{3}}\omega + \ldots, \quad \theta_0 \sim -3\tilde{\tilde{F}}_2 s^{-\frac{1}{3}}\lambda^{-\frac{4}{3}}\phi\omega\epsilon^{\frac{1}{3}}y^{-1} + \ldots, \tag{4.8b, c}$$

where $\omega = -\mathrm{Ai}'(0)$. Hence the flow within the wall-layer region induces the motion of the fluid in the $y = O(1)$ region where u, v, θ are expanded as

$$u = U_0\epsilon^{\frac{1}{3}} + \ldots, \quad v = V_0\epsilon^{-\frac{2}{3}} + \ldots, \quad \theta = \Theta_0\epsilon^{\frac{1}{3}} + \ldots, \tag{4.9a–c}$$

and the Laplace transforms of U_0, V_0 and Θ_0 are found to be given by

$$\tilde{\tilde{U}}_0 = -3\frac{\tilde{\tilde{F}}_1\bar{u}'}{\bar{u}}s^{-\frac{1}{3}}\lambda^{-\frac{1}{3}}\omega m(y,a) + \ldots, \quad \tilde{\tilde{V}}_0 = 3\tilde{\tilde{F}}_1 s^{\frac{2}{3}}\lambda^{-\frac{1}{3}}\omega m(y,a) + \ldots, \tag{4.10a, b}$$

$$\Theta_0 = -3\frac{\tilde{\tilde{F}}_2\bar{T}'}{\bar{u}}s^{-\frac{1}{3}}\lambda^{-\frac{4}{3}}\omega m(y,a) + \ldots, \tag{4.10c}$$

where m is a solution of the stationary Rayleigh equation problem

$$\bar{u}(d_y^2 - a^2)\,m - \bar{u}''m = 0, \tag{4.11a}$$

$$m(0) = 1, \quad m(\infty) = 0. \tag{4.11b}$$

The functions in (4.10) decay to zero exponentially as $y \to \infty$ and satisfy the matching conditions (4.8). We can invert the Laplace transforms and use the large-X form of the velocity and temperature fields as the initial conditions for the solution of the perturbation equations (2.6*b*), (2.6*e*), (2.7) subject to (2.6*f*). For the isolated wall functions $F_{1,2}^+(X) = \delta(X)$, inversion of (4.5) and the corresponding forms for $\tilde{\tilde{u}}_0$ and θ_0 yields the similarity solution

$$u_0 \sim \frac{1}{X}U_A\left(\frac{\xi}{X^{\frac{1}{3}}}\right), \quad v_0 \sim \frac{1}{X^{\frac{2}{3}}}V_A\left(\frac{\xi}{X^{\frac{1}{3}}}\right), \quad \theta_0 \sim \frac{1}{X}\theta_A\left(\frac{\xi}{X^{\frac{1}{3}}}\right), \tag{4.12}$$

where U_A, V_A, θ_A are known functions of $\xi/X^{\frac{1}{3}}$.

We now demonstrate how the similarity solution can be obtained directly from the disturbance equations. The similarity variable is chosen to be $\xi = y(\lambda/\tilde{x})^{\frac{1}{3}}$, where

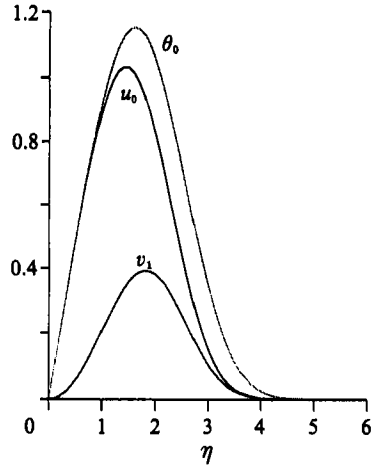

FIGURE 5. The functions u_0, v_1, θ_0 defined by (4.15)–(4.17).

$\tilde{x} = x - \bar{x}$. For $\xi = O(1)$ we expand the perturbed velocity and temperature components as

$$u = \frac{\lambda^{\frac{1}{3}}}{\tilde{x}} u_0(\xi) + \frac{u_1(\xi)}{\tilde{x}^{\frac{1}{3}}} + \ldots, \quad v = \frac{1}{\lambda \tilde{x}^{\frac{4}{3}}} v_0(\xi) + \frac{1}{\lambda \tilde{x}^{\frac{2}{3}}} v_1(\xi) + \frac{1}{\lambda} v_2(\xi) + \ldots, \quad (4.13a, b)$$

$$\theta = \frac{\lambda^{\frac{1}{3}}}{\tilde{x}} \theta_0(\xi) + \frac{\theta_1(\xi)}{\tilde{x}^{\frac{1}{3}}} + \ldots, \quad (4.13c)$$

and impose the wall conditions

$$u_0 = u_0' = v_0 = \theta_0 = \theta_0' = 0, \quad \xi = 0. \quad (4.13d)$$

The above expansions are substituted into (2.7) and at leading order yield

$$v_0'''' + \tfrac{1}{3}\xi^2 v_0''' + \tfrac{7}{3}\xi v_0'' = 0, \quad (4.14)$$

where a prime denotes differentiation with respect to ξ. Equation (4.14) can be solved for v_0'' in terms of Whittaker functions and it can be shown that there exists a solution of (4.14) for which $v_0 = v_0' = \theta, \xi = 0$, and such that at infinity $v_0 \sim 1 +$ exponentially small terms. It is to be noted that the solutions of (4.14) which, for large ξ, behave like ξ and ξ^{-5} terms do not appear in the required solution for v_0. Indeed if these terms did occur the wall-layer solutions could not be matched in the $y = O(1)$ region of the flow. Equations (2.6*b*), (2.6*e*) yield at leading order

$$u_0'' + \tfrac{1}{3}\xi^2 u_0' + \xi u_0 = v_0/\lambda, \quad (1/Pr)\,\theta_0'' + \tfrac{1}{3}\xi^2 \theta_0' + \xi\theta_0 = v_0\phi/\lambda^2. \quad (4.15a, b)$$

The homogeneous forms of (4.15*a*, *b*) have the eigensolutions

$$u_0 = C_1 \xi \exp(-\tfrac{1}{9}\xi^3), \quad \theta_0 = C_2 \xi \exp(-\tfrac{1}{9}Pr\,\xi^3), \quad (4.16)$$

where C_1, C_2 are arbitrary constants. It follows that, since the inhomogeneous solutions of (4.15) must satisfy $u_0 = 0$, $\theta_0 = 0$ at $\xi = 0$, the algebraically decaying solutions of the homogeneous forms of (4.15*a*, *b*) are required. However, if these solutions are retained we cannot match with the core flow, so v_0 must be zero. Hence the highest-order term in the expansion of v is v_1 and (2.7) then gives

$$v_1'''' + \tfrac{1}{3}\xi^2 v_1''' + \tfrac{1}{3}u\xi v_1'' = 2\lambda'\{u_0 + \tfrac{5}{3}\xi u_0' + \tfrac{1}{3}\xi^2 u_0''\}, \quad (4.17)$$

which has the solution $v_1 = \frac{1}{2}\lambda'\xi u_0$ satisfying the boundary conditions. The functions u_0, v_1, θ_0 are shown in figure 5. At leading order in the expansions of u, v and θ it is clear that the disturbed flow is confined to the wall-layer region; however, at next

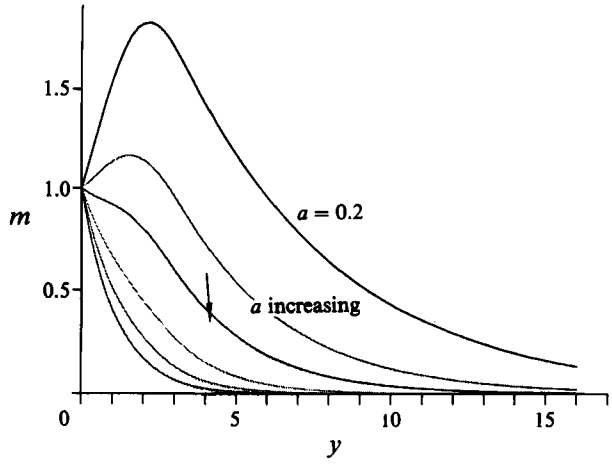

FIGURE 6. The function $m(y)$ for $a = 0.2, 0.3, 0.4, 0.5, 0.6, 0.7$.

order the flow is no longer contained in the wall layer. The function u_1 satisfies the equation

$$u_1'' + \tfrac{1}{3}\xi^2 u_1' + \tfrac{1}{3}\xi u_1 = a^2 u_0/\lambda^{\frac{1}{3}}, \tag{4.18a}$$

and hence

$$u_1 = \frac{-3C_1 a^2}{\lambda^{\frac{1}{3}}}\left\{\exp(-\tfrac{1}{9}\xi^3) - \frac{\hat{u}_1(\xi)}{\hat{u}_1(0)}\right\}, \tag{4.18b}$$

where $\hat{u}_1$ is the exponentially decaying solution of

$$\hat{u}_1'' + \tfrac{1}{3}\xi^2 \hat{u}_1' + \tfrac{1}{3}\xi \hat{u}_1 = 0,$$

and θ_1 is similarly given by

$$\theta_1 = \frac{-3C_2 a^2}{Pr\lambda^{\frac{1}{3}}}\left\{\exp(-\tfrac{1}{9}\xi^3 Pr) - \frac{\hat{\theta}_1(\xi)}{\hat{\theta}_1(0)}\right\}. \tag{4.19}$$

Here $\hat{\theta}_1$ is the exponentially decaying solution of

$$\frac{1}{Pr}\hat{\theta}_1'' + \tfrac{1}{3}\xi^2 \hat{\theta}_1' + \tfrac{1}{3}\xi \hat{\theta}_1 = 0.$$

At higher order v_2 is found to satisfy

$$(d_\xi^2 + \tfrac{1}{3}\xi^2 d_\xi + \tfrac{2}{3}\xi)\, v_2'' = \frac{2\lambda'}{3\lambda^{\frac{1}{3}}}(u_1 + 3\xi u_1' + \xi^2 u_1'') + \frac{a^2}{\lambda^{\frac{2}{3}}}(2v_1'' + \tfrac{1}{3}\xi^2 v_1' + \tfrac{2}{3}\xi v_1). \tag{4.20}$$

Equation (4.20) is solved subject to the boundary conditions $v_2 = v_2' = 0$, $\xi = 0$ and $\xi =$ constant + exponentially small terms as $\xi \to \infty$. Integration of (4.20) numerically shows that this constant is non-zero, hence the perturbed velocity and temperature fields for the $y = O(1)$ region are of the form

$$u \sim -\frac{C_1 \tilde{x}\overline{u}'}{\overline{u}} m(y,a), \quad v \sim m(y,a), \quad \theta \sim -\frac{C_2 \tilde{x}\overline{T}'}{\overline{u}} m(y,a), \tag{4.21}$$

where m satisfies (4.11). Hence it follows that $(u, v, \theta) \to 0$ as $y \to \infty$. The function $m(y,a)$ is shown in figure 6 for different vortex wavenumbers. By combining (4.13), (4.20) a composite disturbance field is obtained for some small value of $\tilde{x}$ which can be

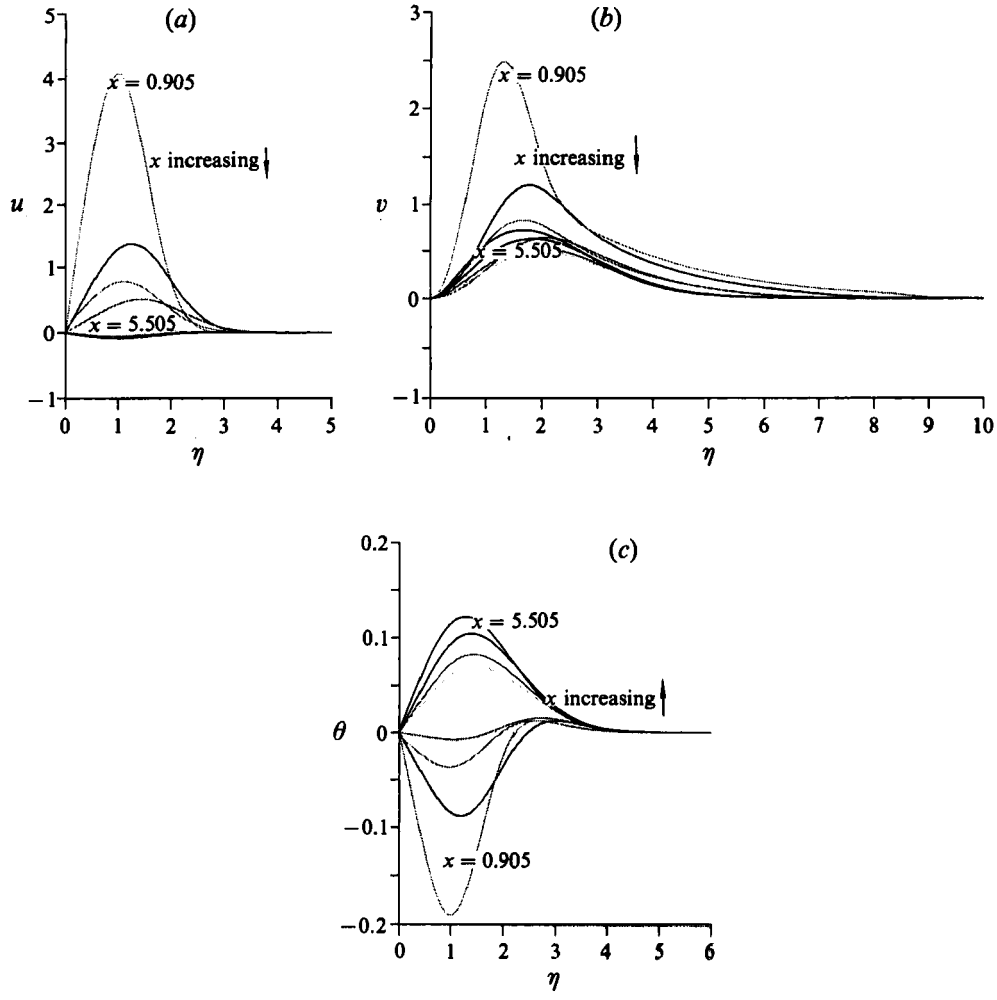

FIGURE 7 (*a–c*). The downstream development of the functions u, v, w associated with (4.22); the curves shown correspond to values of x varying between 0.905 and 5.505 in steps of 0.66.

used as the initial condition for the solution of the full linear disturbance equations (2.6*b*), (2.6*e*), (2.7), subject to the boundary conditions (2.6*f*).

The calculations we now report on were carried out using the numerical scheme described earlier with the starting point of the calculation at $x = 0.505$ and with the stepsize in the x-direction, $\bar{\epsilon}$, equal to 0.004. In order to determine the effects of the wall forcing functions, imposed at the position $\bar{x} = \frac{1}{2}$, on the flow downstream of that point the pseudoenergy $E(x)$ of the flow was monitored where

$$E = \int_0^\infty \{u^2(x,y) + v^2(x,y) + w^2(x,y)\}\,\mathrm{d}y$$

and the local growth rate $\bar{\sigma}(x) = (\partial E/\partial x)/E$. The position of neutral stability is defined as the position at which $\bar{\sigma} = 0$. Of course other instability criteria can be defined but some limited experimentation showed that the neutral curve is not greatly dependent on the choice of flow property used to monitor the growth of the disturbance. Moreover, we believe that the flow property we have used is a sensible

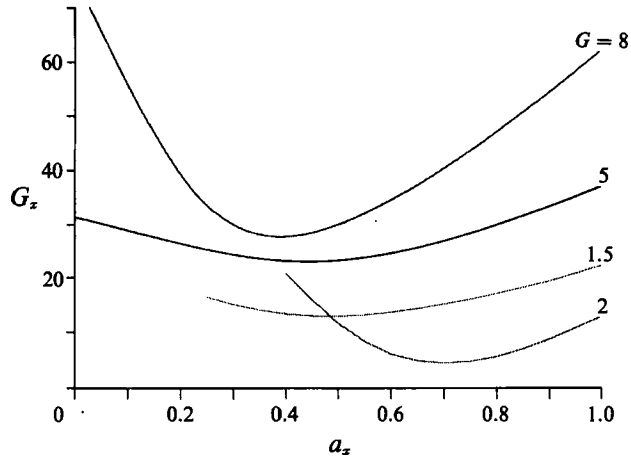

FIGURE 8. The neutral curves corresponding to the downstream development shown in figure 7.

one because it accounts for the changes in all of the velocity components in some sense averaged across the flow field. For a given wall forcing function, G and different values of a the disturbance equation was marched downstream and the position at which the vortex structure began to grow was calculated. The local wavenumber a_x and the local Grashof number G_x were calculated and a neutral curve in (a_x, G_x) space formed. This process was repeated for different values of G. Two sets of initial conditions were considered. First the problem was solved for an initial disturbance of the form

$$u = \xi \exp(-\tfrac{1}{9}\xi^3), \quad v = -\tfrac{1}{2}\xi\lambda' u, \quad \theta = 0 \quad \text{imposed at} \quad x = \bar{x} + 0.005. \quad (4.22)$$

This type of disturbance corresponds to the situation when the vortices are stimulated by wall roughness; later we shall look at the case when the vortices are induced by non-uniform wall heating.

The development of the velocity and temperature fields downstream is shown in figure 7 (a–c) for $G = 5, a = 0.4$. The corresponding neutral curves for the problem are shown in figure 8. We see that, as G varies, the neutral curves move around in the wavenumber–Grashof number plane. Our calculations show that there is a neutral curve corresponding to G near 2 which has the lowest minimum. Furthermore the minimum value of the Grashof number on that curve is about 4. When the Grashof number is increased or decreased from this value the curves move upwards, so the flow is more stable. It should be noted that the effect of changing G in the calculation of the neutral curves shown in figure 8 is exactly equivalent to calculations carried out with a fixed G but with the position where the forcing begins now being varied. Thus in figure 8 increasing G corresponds to moving the forcing further downstream from the leading edge. In that case it is not surprising that the curves in the (a_x, G_x)-plane move upwards since the forcing cannot initially generate an unstable vortex since the form of the initial disturbance is not typical of a growing vortex flow. Likewise when G is decreased in figure 8 the forcing is being moved progressively towards the leading edge; the fact that the curves move upwards in this case again implies that roughness near the edge has a relatively weak effect on the flow. In an experiment one would expect that localized roughness elements would be distributed at several sites along the wall so that the most dangerous mode would be the one excited. We postpone a discussion of the available experimental results until the final section of this paper.

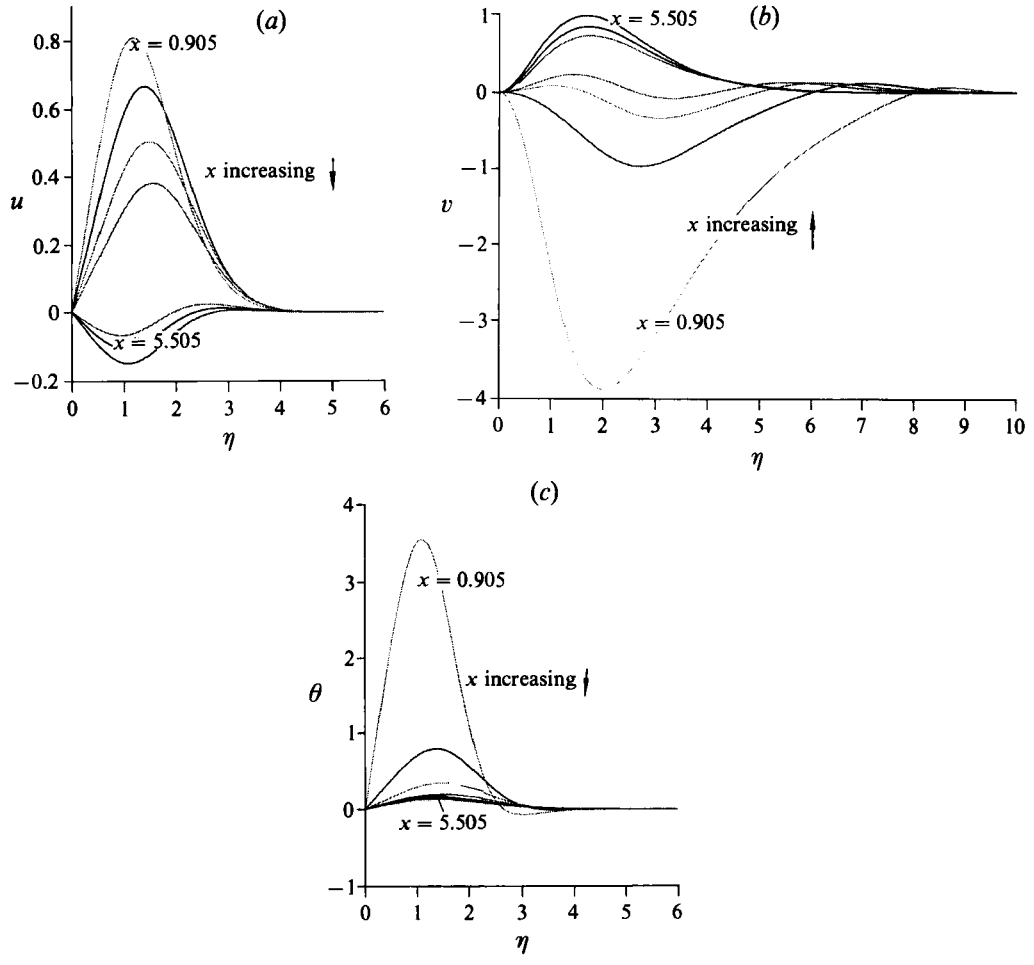

FIGURE 9(*a–c*). The downstream development of the functions u, v, w associated with (4.23); the curves shown correspond to values of x varying between 0.905 and 5.505 in steps of 0.66.

In fact the discussion given above applies equally well to the case when the forcing corresponds to a localized temperature variation at the plate. In particular for the problem with

$$u = 0, \quad v = \tfrac{1}{2}\xi\lambda'(\xi\exp(-\tfrac{1}{9}\xi^3)), \quad \theta = \xi\exp(-\tfrac{1}{9}\xi^3 Pr) \quad \text{imposed at} \quad x = \bar{x}+0.005 \tag{4.23}$$

we now find that the most dangerous disturbance occurs when G is close to 8 whilst the local Grashof number corresponding to this most dangerous mode is about 2. The downstream development of the velocity and temperature fields is shown in figure 9(*a–c*). The corresponding neutral curves are shown in figure 10. Again for large values of G we can see that the forcing applied does not initially generate unstable vortex structures. It is also clear that the forcing becomes less dangerous when it is moved close to the leading edge. In each of the above calculations it was found that the dimensionless energy E decreases by several orders of magnitude before the growth rate $\bar{\sigma}$ becomes positive. This means that the forcing applied generates vortices which decay significantly before they begin to grow. Hence a localized wall forcing function is not a particularly efficient means for the production of longitudinal

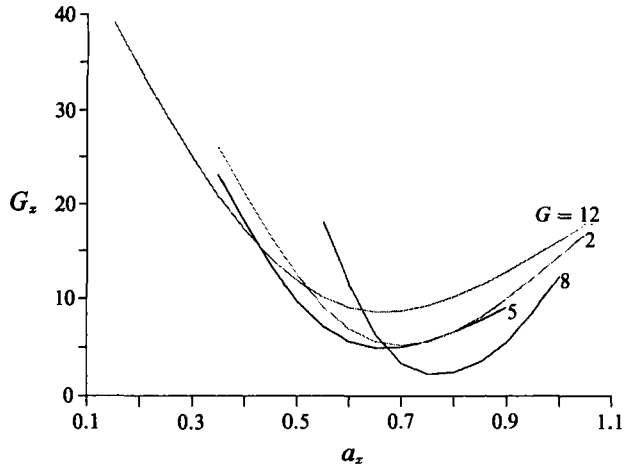

FIGURE 10. The neutral curves corresponding to the downstream development shown in figure 9.

vortices. However, note that, despite being an inefficient generator of longitudinal vortex rolls, in the absence of other forcing modes an isolated wall-heating forcing will result in vortex growth downstream. We conclude this section by noting that if instability is caused by isolated wall roughness or non-uniform wall heating then we expect instability to occur when the local Grashof number exceeds about 2.

5. Free-stream disturbances

We shall now consider the generation of vortex structures due to a free-stream longitudinal vortex field impinging on the leading edge rather than imposing some initial disturbance on the flow. This analysis closely follows the work of Hall (1990) on the receptivity problem for Görtler vortices.

We take the stream velocity component to be of the form

$$u = 1 + \Delta\, \mathrm{e}^{\mathrm{i}az} u_{\mathrm{c}}(y), \quad x = 0, \tag{5.1}$$

and hence we have assumed a dependence of the impinging vortex structure on the boundary-layer lengthscale. However it will later be shown that the case of u_{c} independent of y gives rise to the most dangerous vortex mode. We consider u_{c} to be of the form $u_{\mathrm{c}}(y) = \cos(by + \phi)$, where b and ϕ are constants so that the disturbance is periodic in both the y- and z-directions. We need to consider two regions, the boundary layer $y \sim x^{\frac{1}{2}}$ and also an outer region $y \sim O(1)$. This is because the wavelengths in the spanwise and normal directions are large compared with the boundary-layer scale $x^{\frac{1}{2}}$.

Consider the boundary-layer region $y \sim x^{\frac{1}{2}}$ with $x \ll 1$ and allow $y/x^{\frac{1}{2}} \to \infty$. The disturbance equations (2.6), (2.7) may be written in the form

$$\left\{\partial_y^2 - a^2 - \partial_x - \frac{\beta}{(2x)^{\frac{1}{2}}}\partial_y\right\} u = 0, \qquad \left\{\frac{\partial_y^2}{Pr} - \frac{a^2}{Pr} - \partial_x - \frac{\beta}{(2x)^{\frac{1}{2}}}\partial_y\right\}\theta = 0, \tag{5.2a, b}$$

$$\left\{\partial_y^2 - a^2 - \partial_x - \frac{\beta}{(2x)^{\frac{1}{2}}}\partial_y\right\}\{\partial_y^2 - a^2\} v = a^2 G\theta + \frac{\beta}{(2x)^{\frac{3}{2}}} u_{yy} + \frac{a^2\beta u}{(2x)^{\frac{3}{2}}}, \tag{5.2c}$$

where

$$\beta = \lim_{\eta \to \infty} (\eta f' - f), \tag{5.3}$$

is the Blasius constant.

We require a solution of (5.2*a–c*) which will maintain the periodicity $2\pi/b$ in the y-direction, and hence we take

$$u = u_{\mathrm{p}} = \mathrm{e}^{-\nu_1^2 x}\cos(by+\phi-b\beta(2x)^{\frac{1}{2}}), \quad \theta = \theta_{\mathrm{p}} = \theta_1\,\mathrm{e}^{(-\nu_1^2 x/Pr)}\cos(by+\phi-b\beta(2x)^{\frac{1}{2}}), \tag{5.4a, b}$$

$$v = v_{\mathrm{p}} = \left\{\left[\frac{\beta(b^2-a^2)}{\nu_1^2(2x)^{\frac{1}{2}}}+k_1\right]\mathrm{e}^{-\nu_1^2 x} - \frac{a^2G\theta_1 Pr}{\nu^4(1-Pr)}\mathrm{e}^{-\nu_1^2 x/Pr}\right\}\cos(by+\phi-b\beta(2x)^{\frac{1}{2}}) \quad \text{for} \quad Pr \neq 1, \tag{5.4c}$$

$$v = v_{\mathrm{p}} = \left\{\frac{1}{\nu_1^2}\left(a^2G\theta_1 x+\frac{\beta(b^2-a^2)}{(2x)^{\frac{1}{2}}}\right)+k_2\right\}\mathrm{e}^{-\nu_1^2 x}\cos(by+\phi-b\beta(2x)^{\frac{1}{2}}) \quad \text{for} \quad Pr = 1, \tag{5.4d}$$

where $\nu_1^2 = a^2+b^2$ and θ_1, k_1 and k_2 are arbitrary constants. Note that the exponential functions of x appearing above should also be formally expanded in powers of x but it is more convenient to not do so and use the equally accurate forms given above.

There is an eigensolution of (5.2*c*), $v = Q(x)\,\mathrm{e}^{-ay}$, for arbitrary $Q(x)$ and this solution is needed in order to match with the boundary-layer solution. Hence the appropriate solution of (5.2*c*) is

$$v = v_{\mathrm{p}} + Q(x)\,\mathrm{e}^{-ay}, \tag{5.5}$$

and it is to be noted that the boundary-layer structure causes the periodic form of v to occur only when $ay \gg 1$. For the region where $x = O(1)$ and $ay \gg 1$, at the edge of the boundary layer, we must solve the disturbance equations subject to

$$(u, v, \theta) = (u_{\mathrm{p}}, v_{\mathrm{p}}, \theta_{\mathrm{p}}). \tag{5.6}$$

We now consider the $\eta = O(1)$ region with $x \ll 1$ and we determine $Q(x)$ by matching with the boundary-layer solution. The functions u, v and θ are obtained from expansions in powers of $x^{\frac{1}{2}}$ in the disturbance equations by perturbing the basic flow in the form

$$u = \cos\phi\{\bar{f}'+\eta/2\bar{f}''\}+\ldots, \quad \theta = \cos\phi\{h'+\eta/2h''\}+\ldots, \tag{5.7a, b}$$

$$v = \frac{\cos\phi}{(2x)^{\frac{1}{2}}}\{\tfrac{1}{2}(\eta\bar{f}'-f)+\eta^2/2\bar{f}''\}+\ldots, \tag{5.7c}$$

where $h(\eta)$ satisfies $h''' = -Pr\bar{f}h''$, (5.7*d*)

and, as $\eta\to\infty$, $v\to\cos\phi\beta/[2(2x)^{\frac{1}{2}}]$. (5.8)

Matching with the boundary-layer solution for $\eta \gg 1$ yields

$$Q+\cos\frac{(\phi-b\beta(2x)^{\frac{1}{2}})}{\nu_1^2}\left[\left\{\frac{(b^2-a^2)}{(2x)^{\frac{1}{2}}}\beta+k_3\right\}\mathrm{e}^{-\nu_1^2 x}+\frac{a^2G\theta_1 Pr}{\nu_1^2(Pr-1)}\mathrm{e}^{-\nu_1^2 x/Pr}\right] = \frac{\beta\cos\phi}{2(2x)^{\frac{1}{2}}}. \tag{5.9}$$

A composite solution is formed, from the $y\sim x^{\frac{1}{2}}$ and $y\sim O(1)$ solutions, for small x to give the asymptotic forms for u, v and θ, and hence initial data for the solution of the disturbance equations using the numerical scheme starting at a small value of x.

We note that when $\phi = 0$, the function u_{c} takes the form $u_{\mathrm{c}} = \cos(by)$ which means that the incoming vortex field does not satisfy the no-slip condition at the wall. Hence we choose ϕ to be zero since this relates to the most physically relevant case corresponding to $u_{\mathrm{c}}(0) \neq 0$. We again monitored the dimensionless energy $E(x)$ of the flow where

$$E = \int_0^\infty \{u^2(x,y)+v^2(x,y)+w^2(x,y)\}\,\mathrm{d}y,$$

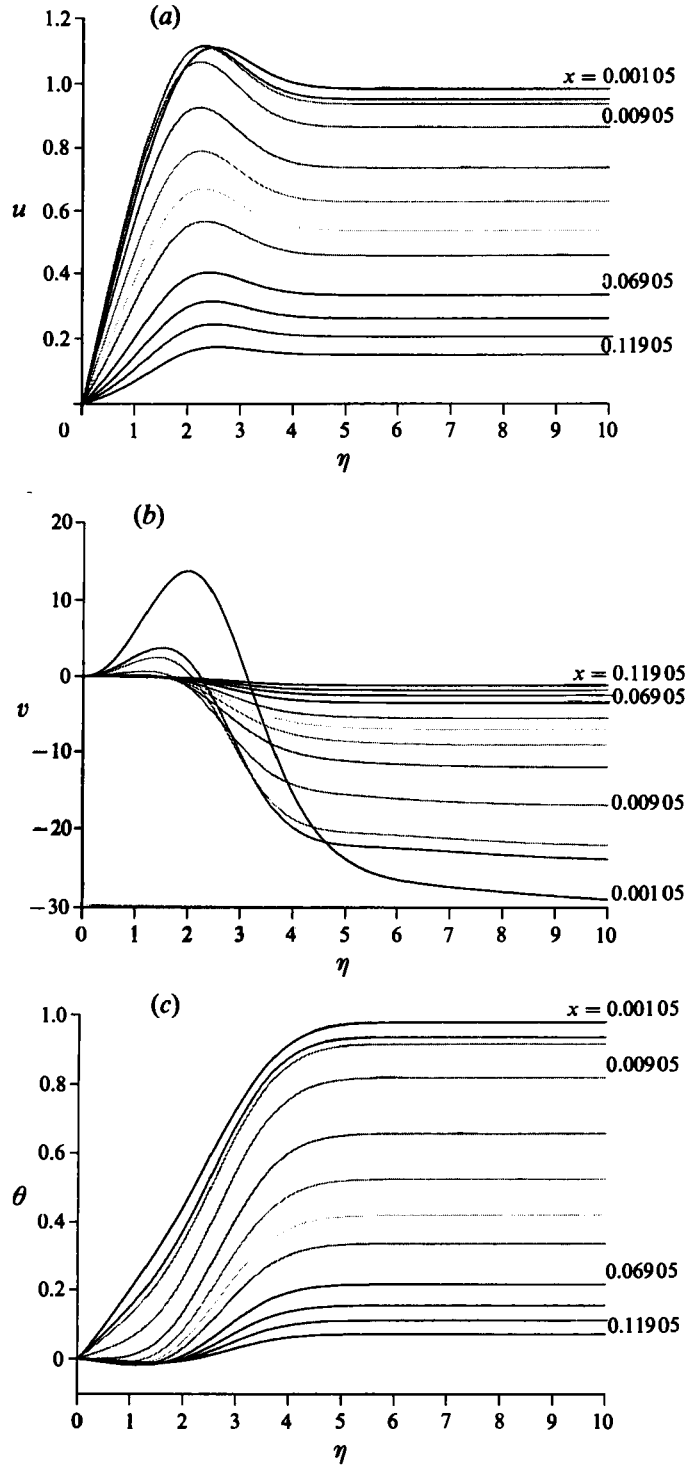

FIGURE 11 (*a–c*). The downstream development of u, v, θ for the free-stream receptivity problem.

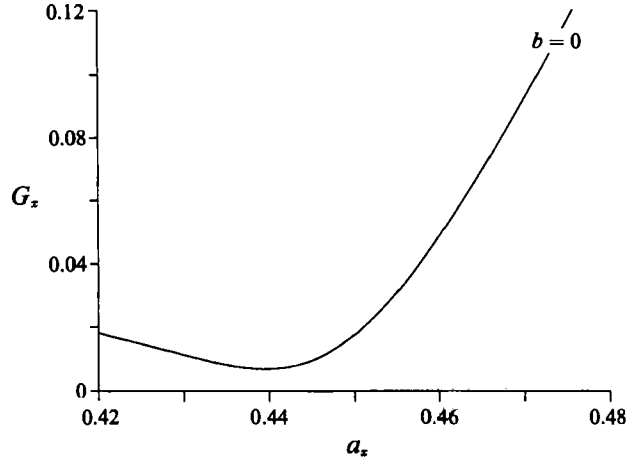

FIGURE 12. The neutral curve for the free-stream receptivity problem with $b = 0$.

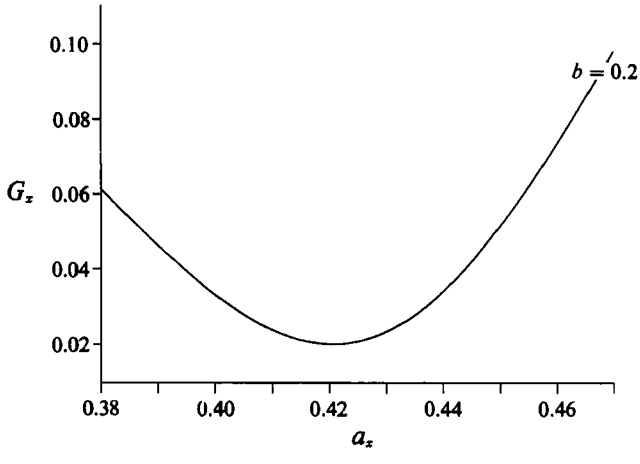

FIGURE 13. The neutral curve for the free-stream receptivity problem with $b = 0.2$.

and the local growth rate $\bar{\sigma}(x) = (\partial E/\partial x)/E$. The position of neutral stability is defined as the position at which $\bar{\sigma} = 0$.

For the receptivity problem formulated above, the disturbance equations were marched downstream using the numerical scheme described in §3. The steplength in the streamwise direction was taken to be 0.00001, this very small value being necessary, in the numerical scheme chosen, owing to the singular behaviour of v and x.

The profiles for the disturbance velocity and temperature components as the vortex develops downstream are shown in figure 11 (a–c). We can see that the edge velocity for the streamwise velocity component decreases monotonically with x as does the temperature component. The normal velocity component v at the edge of the boundary layer is seen to increase as we move downstream; however, for larger values of x the edge velocity begins to decrease with x owing to the exponential factor in (5.4c). In figures 12 and 13 the local Grashof number and the local wavenumber have been calculated at the points of neutral stability where the local growth rate vanishes; this enables us to generate neutral curves in the local wavenumber – Grashof number space. For these two cases the parameters chosen were $G = 70$,

$\theta_1 = 1$. We conclude from these calculations that instability first occurs when $b = 0$; in fact further calculations for different values of b produced neutral curves located above that for $b = 0$. We deduce that $u_c \sim \cos az$ is the most dangerous form for the incoming vortex field. We conclude from figure 12 that free-stream disturbances are able to cause the onset of instability when the local Grashof number is bigger than about 0.02; this is significantly lower than the critical Grashof number associated with isolated wall forcing.

6. Distributed roughness

We shall now consider the effects of wall heating on the forced-convection flow when the wall forcing is described by a non-localized forcing function and occurs on an $O(1)$ streamwise lengthscale. Again we concentrate on the $O(1)$ wavenumber regime. The linearized disturbance equations (2.6*b*), (2.6*e*), (2.7) were solved together with the boundary conditions (2.6*f*), where $F_1(x)$ is given by

$$F_1(x) = 40(x-\tfrac{1}{2})\,\mathrm{e}^{-20(x-1/2)^2}, \quad x \geqslant \tfrac{1}{2}, \tag{6.1}$$

and $F_2 = 0$ so that the vortex is induced by wall roughness rather than non-uniform wall heating. Given a function $q(a)$ the disturbance equations can be marched downstream from $x = 0$ for various values of a using the numerical scheme described in §3 with no initial disturbance. We then invert this transformed flow field in (a, x, y)-space to give the flow field in (z, x, y)-space induced by a forcing function of height proportional to $\tilde{q}(z)$, the inverse Fourier transform of $q(a)$. A symmetric obstacle $\tilde{q}(z)$ was considered with

$$\tilde{q}(z) = \tfrac{1}{4}\pi^{\frac{1}{2}} \exp(-\tfrac{1}{16}z^2), \tag{6.2}$$

and $q(a)$, the Fourier transform of (6.2), is given by

$$q(a) = \tfrac{1}{2}\exp(-4a^2). \tag{6.3}$$

We then combine (6.1) and (6.3) to give the boundary conditions (2.6*f*) in (a, x, y)-space. The disturbance equations were marched downstream and $\theta^*(a, x, y)$, the maximum value of θ, was calculated. This procedure was repeated for various values of a and the transform in z was then inverted numerically to give $\tilde{\theta}^*(z, x, y)$. The parameters chosen were x varying between 0 and 10 whilst z varies between 0 and 10. The calculation was repeated for different values of the Grashof number G.

The velocity and temperature profiles for the symmetric obstacle are shown in figure 14(*a–c*) for $G = 8, a = 0.45$. Note that the maximum value of θ occurs initially at the wall and, as x increases, its position moves away from the wall.

For a distributed wall forcing function there is a strong coupling between the induced vortex field and the wall forcing, with the ratio between the two being a function of the wavenumber and the Görtler number. In principle we could maximize the coupling between the vortex field and the forcing by varying a and G though this would require a large amount of computer time.

The contours of $\tilde{\theta}^*(z, x, y)$ are shown in figure 15(*a–d*), demonstrating that immediately after the obstacle the perturbed temperature field decays and is formed into a wake solution behind the obstacle. However, further downstream the effects of thermal instability due to the heated wall reamplifies this disturbance into longitudinal vortex rolls. The distance between the reamplification of the disturbance and the obstacle decreases as we increase the Grashof number. The same effect could have been demonstrated by following the same method as in §5 by fixing the Grashof number and varying the position at which the forcing was first applied.

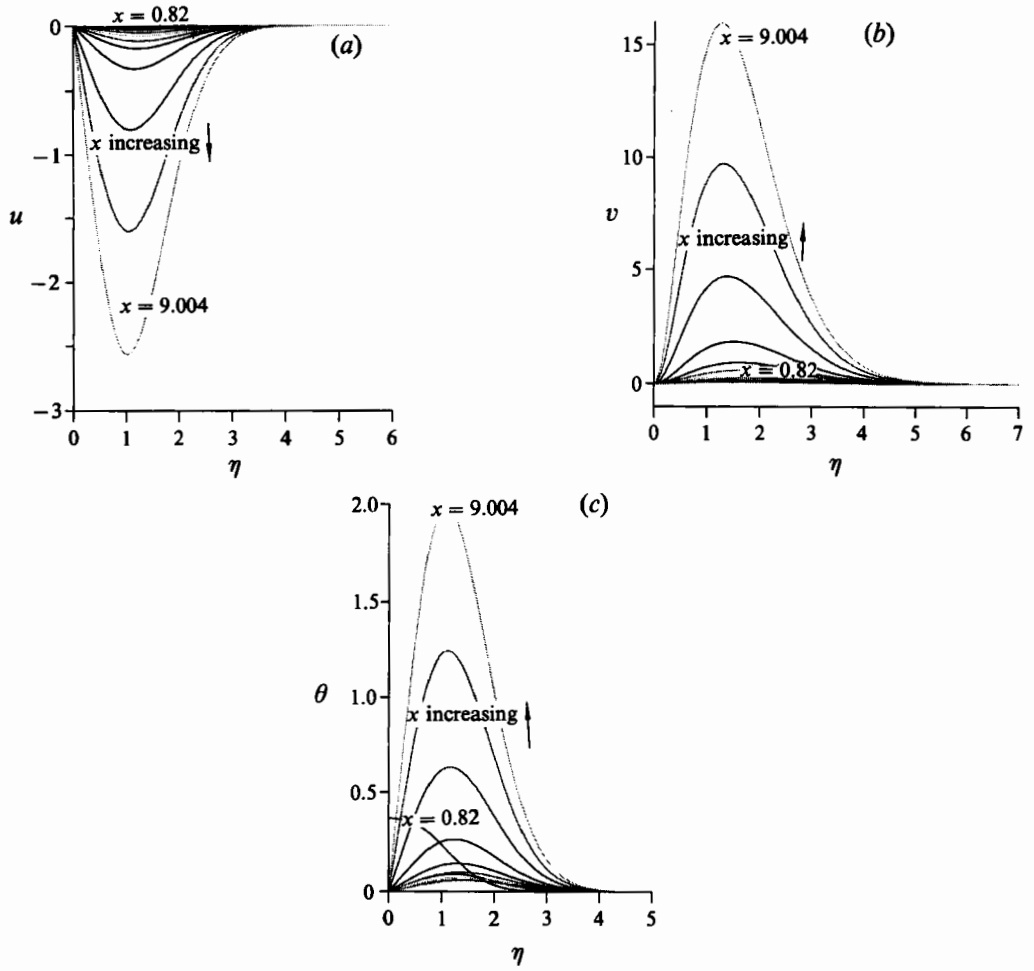

FIGURE 14(*a–c*). The development of u, v, θ for the obstacle given by (6.1). The results shown correspond to $G = 8, a = 0.45$.

The same calculations were repeated for an asymmetric obstacle of the form

$$\tilde{q}(z) = \tfrac{1}{13}\pi^{\frac{1}{2}} z \exp(-\tfrac{1}{16}z^2). \tag{6.4}$$

The results are shown in figure 16(*a–d*). A similar flow structure to that of the symmetric obstacle was observed with the perturbed flow field formed into a wake before subsequently being reamplified further downstream into longitudinal vortex roll structures. Again the distance of the resulting vortex structure from the leading edge is dependent upon the Grashof number. Note that similar flow structures have been reproduced experimentally by Mangalam, Dagenhart & Meyers (1991) for the analogous Görtler-type vortex problem.

7. The high-Grashof-number limit and the fastest growing mode

At high values of the Grashof number we expect that viscous effects will be negligible except at low or high vortex wavenumbers. We follow the approach of Denier *et al.* (1991) who consider the most unstable Görtler vortex. An examination

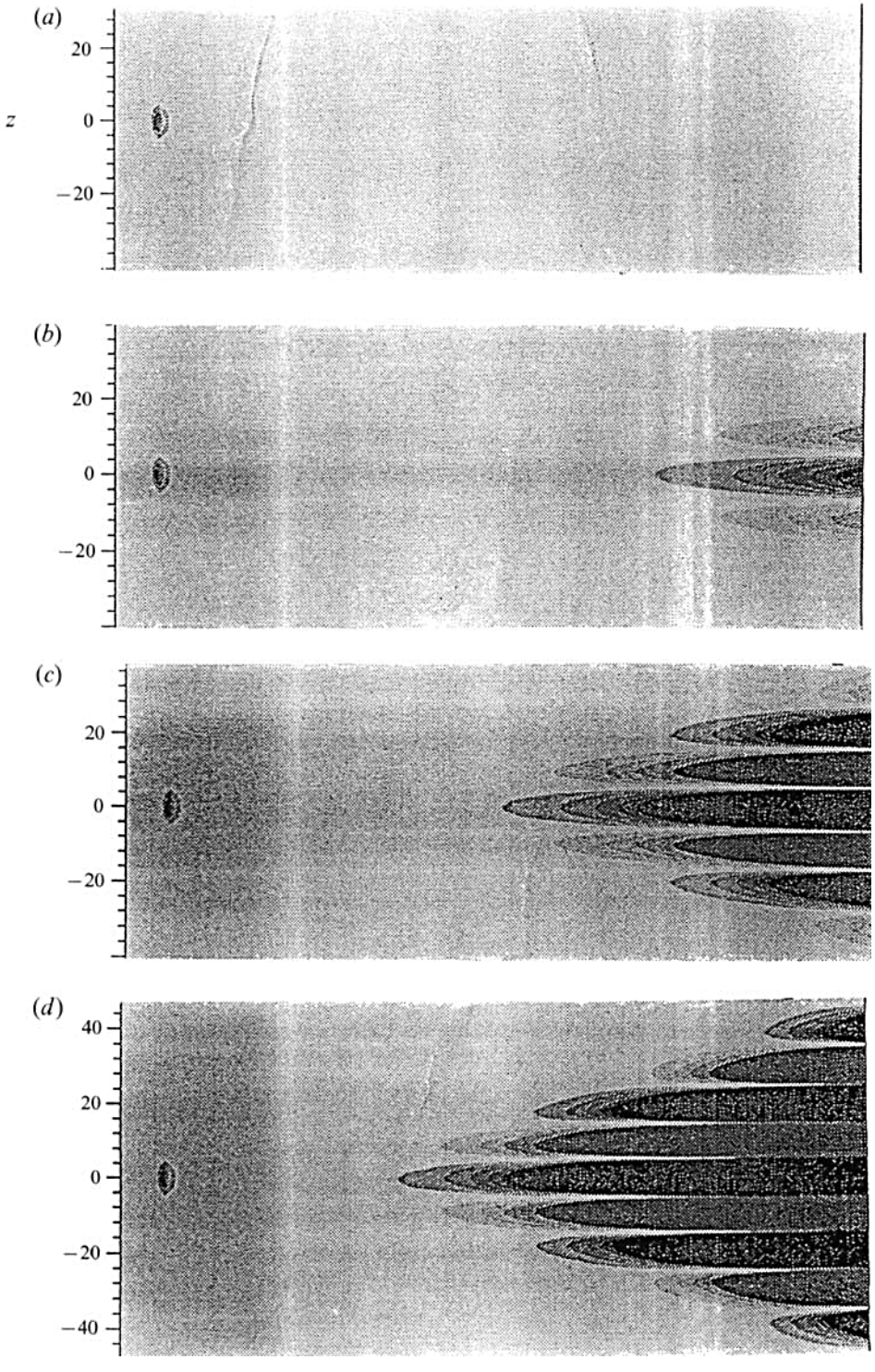

FIGURE 15. Contours of constant $\tilde{\theta}^*$ for the obstacle given by (6.1), (6.2) for (*a*) $G = 2$, (*b*) $G = 5$, (*c*) $G = 8$, (*d*) $G = 12$.

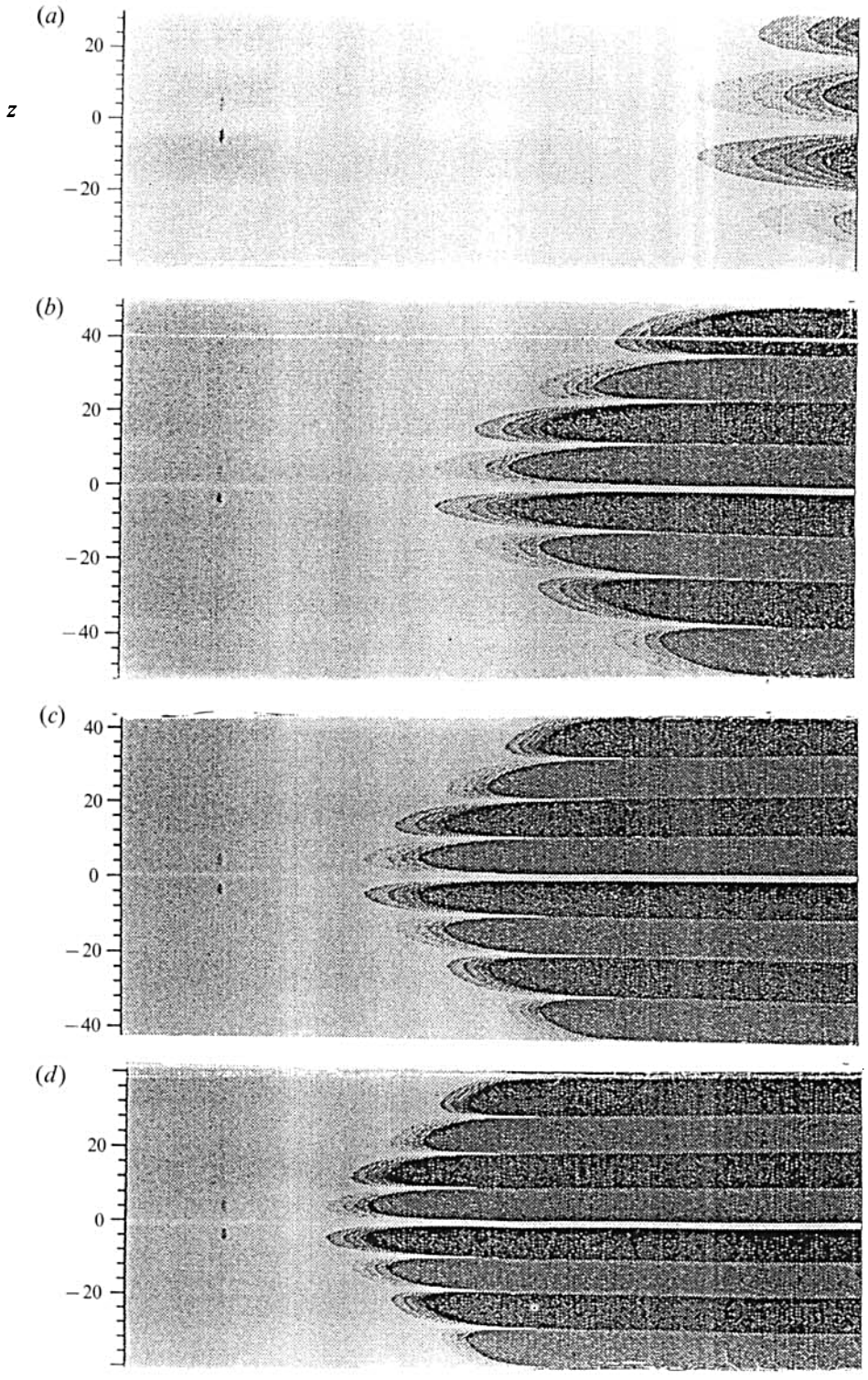

FIGURE 16. Contours of constant $\tilde{\theta}^*$ for the obstacle given by (6.1), (6.4) for (*a*) $G = 2$, (*b*) $G = 5$, (*c*) $G = 8$, (*d*) $G = 12$.

of (2.6) for $G \gg 1$ with a held fixed suggests that inviscid disturbances have $\partial_x \sim G^{\frac{1}{2}}$; we are therefore led to the expansions

$$[u, G^{-\frac{1}{2}}v, G^{-\frac{1}{2}}w, G^{-1}p, \theta] = [(u_0, v_0, w_0, p_0, \theta_0) + \ldots] \exp \int^x G^{\frac{1}{2}} \hat{\beta}(x)\, \mathrm{d}x, \tag{7.1}$$

where u_0, v_0, etc. are functions of x and y only whilst $\hat{\beta}$ expands as

$$\hat{\beta} = \hat{\beta}_0 + \hat{\beta}_1 G^{-\frac{1}{2}} + \ldots. \tag{7.2}$$

If the above expansions are substituted into (2.6) and the dominant terms are retained in the limit $G \to \infty$ we obtain

$$\hat{\beta}_0 u_0 + v_{0y} + \mathrm{i}a w_0 = 0, \quad \hat{\beta}_0 \bar{u} u_0 + v_0 \bar{u}_y = 0, \tag{7.3a, b}$$

$$\hat{\beta}_0 \bar{u} v_0 = -p_{0y} + \theta_0, \quad \hat{\beta}_0 \bar{u} w_0 = -\mathrm{i}a p_0, \quad \hat{\beta}_0 \bar{u} \theta_0 + v_0 \bar{T}_y = 0, \tag{7.3c–e}$$

and we can eliminate u_0, w_0, p_0 and θ_0 from this system to give

$$\bar{u}[v_{0yy} - a^2 v_0] - \bar{u}_{yy} v_0 = (a^2 \bar{T}_y / \hat{\beta}_0^2 \bar{u})\, v_0. \tag{7.4}$$

This equation must be solved subject to $v_0 = 0$ at $y = 0, \infty$ and this specifies an eigenvalue problem $\hat{\beta}_0 = \hat{\beta}_0(a)$.

Thus in the inviscid limit the growth of the disturbance is governed by a quasi-parallel stability problem since in that case the disturbance varies on a relatively short, $G^{-\frac{1}{2}}$, lengthscale in the x-direction. We shall restrict our attention here to the determination of $\hat{\beta}_0$; higher-order terms in the expansion of the growth rate can be obtained in a routine manner. Note that we have assumed that there are unstable solutions of (7.4); this is assured if there are regions where $\bar{T}_y < 0$ in $0 < y < \infty$. The numerical solution of the eigenvalue problem specified by (7.4) together with the conditions $v_0 = 0, y = 0, \infty$ is made non-trivial because of the singularity in the equation at $y = 0$. An examination of (7.4) for $y \ll 1$ shows that for $y \ll 1, v_0 \sim y^{\frac{3}{2}}$. In fact (7.4) is more easily solved by making the transformation $\eta = (1/\bar{u}_y(x, 0)) \log y$ and the results presented below were obtained using that transformation.

In figure 17 we show the most unstable eigenvalue for $Pr = 1$. It can be seen that the growth rate increases monotonically with a. The eigenvalue shown is in fact just one of an infinite sequence of unstable modes. For small a we see that the growth rate goes to zero like some power of a; actually our calculations suggest that $\hat{\beta}_0 \sim a^{\frac{1}{2}}$ for $a \ll 1$ and this asymptotic limit will be considered later in this section. In figure 18 we show $v_0(y)$ for three different values of a; note that the disturbance becomes less concentrated as a decreases. Now we investigate further the inviscid problem at large wavenumbers. This will enable us to identify the scale on which viscous effects come into play and therefore we will be in a position to identify the fastest growing mode.

For large values of a the terms $v_{0yy}, a^2 v_0$ in (7.4) are comparable in a thin sublayer of thickness a^{-1}. We shall therefore seek a solution of (7.4) within a layer of depth a^{-1} at the boundary; we therefore define

$$\zeta = ay, \tag{7.5}$$

and note that $\bar{u}, \bar{T}$ expand as

$$\bar{u} = \mu \zeta a^{-1} + \ldots, \quad \bar{T} = 1 - w \zeta a^{-1} + \ldots. \tag{7.6a, b}$$

In order that the dominant terms on the left-hand side of (7.4) are comparable with the term on the right-hand side we must write

$$\hat{\beta}_0 = a \hat{\beta}_{00} + \ldots. \tag{7.7}$$

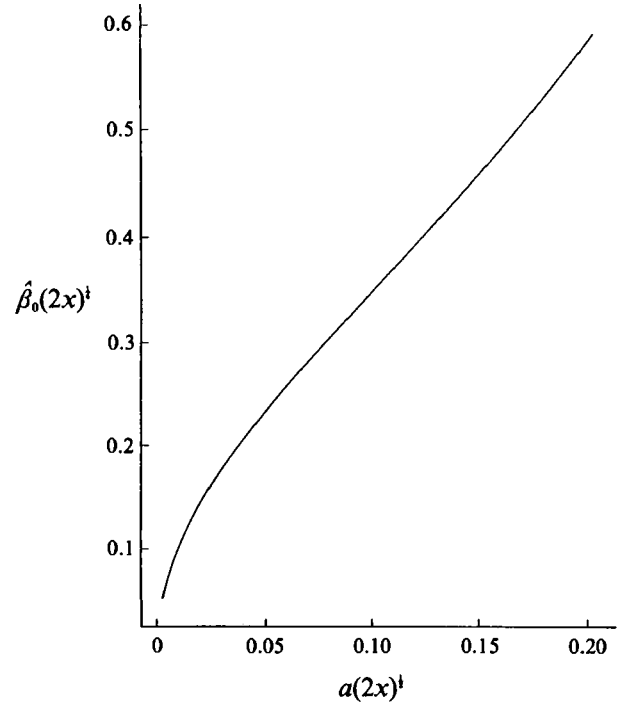

FIGURE 17. The most unstable inviscid eigenvalue associated with (7.4).

The zeroth-order approximation to the eigenvalue problem for $\hat{\beta}_0$ then reduces to

$$(\hat{\beta}_{00}^2\mu^2/\omega)\{v_{0\zeta\zeta}-v_0\} = -v_0\zeta^{-2}, \quad v_0 = 0, \quad \zeta = 0, \infty. \tag{7.8}$$

The solution of (7.8) can be expressed in terms of modified Bessel functions of imaginary order. Since our primary aim at this stage is to see how viscous effects come into play it is not necessary for us to solve (7.8); in fact we can, if necessary, infer the value of $\hat{\beta}_{00}$ from the limiting small-wavenumber approximation to the viscous calculations to be discussed next.

The large-a inviscid analysis given above must, of course, break down when $\bar{u}\,\partial_x \sim \partial y^2$ in which case viscous effects cannot be ignored. This balance is achieved where $a \sim G^{\frac{1}{4}}$ so we now write

$$a = G^{\frac{1}{4}}\hat{a},$$

and modify (7.1) to give

$$[u, G^{-\frac{1}{2}}v, G^{-\frac{1}{2}}w, G^{-\frac{3}{4}}p, \theta] = [(\hat{u}_0, \hat{v}_0, \hat{w}_0, \hat{p}_0, \hat{\theta}_0)+\ldots]\exp\int^x G^{\frac{3}{4}}\hat{\beta}\,\mathrm{d}x, \tag{7.9}$$

where $\hat{u}_0, \hat{v}_0$, etc. are functions only of x and ζ defined by (7.5). The eigenvalue $\hat{\beta}$ now expands as

$$\hat{\beta} = \hat{\beta}_0 + \hat{\beta}_1 G^{-\frac{1}{4}} + \ldots, \tag{7.10}$$

and the zeroth-order growth rate is found to be determined by the eigenvalue problem

$$\hat{\beta}_0\hat{u}_0 + \hat{a}\hat{v}_{0\zeta} + \mathrm{i}\hat{a}\hat{w}_0 = 0, \tag{7.11a}$$

$$\mathscr{L}\hat{u}_0 = \frac{\mu}{\hat{a}^2}\hat{v}_0, \quad \mathscr{L}\hat{v}_0 = \frac{1}{\hat{a}}\hat{p}_{0\zeta} - \frac{\hat{\theta}_0}{\hat{a}^2}, \quad \mathscr{L}\hat{w}_0 = \frac{\mathrm{i}}{\hat{a}}\hat{p}_0, \quad \mathscr{N}\hat{\theta}_0 = \frac{-Pr\omega}{\hat{a}^2}\hat{v}_0, \tag{7.11b–e}$$

$$\hat{u}_0 = \hat{v}_0 = \hat{w}_0 = \hat{\theta}_0 = 0, \quad \zeta = 0, \infty. \tag{7.11f}$$

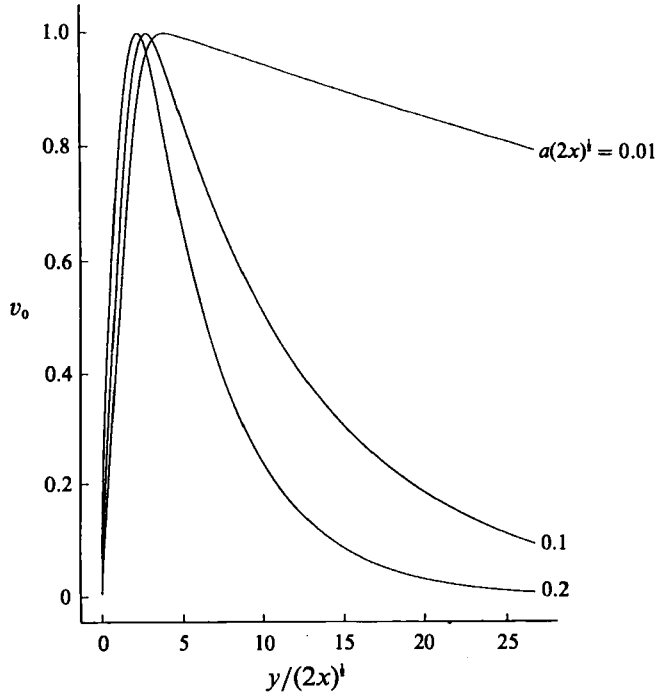

FIGURE 18. The eigenfunctions associated with (7.4) for different values of the wavenumber.

Here the operators $\mathscr{L}$ and $\mathscr{N}$ are defined by

$$\mathscr{L} \equiv \partial_\zeta^2 - 1 - (\mu\zeta/\hat{a}^3)\hat{\beta}_0, \quad \mathscr{N} = \partial_\zeta^2 - 1 - Pr\mu\zeta/\hat{a}^3\,\hat{\beta}_0.$$

A more convenient form of the disturbance equations can be obtained by eliminating $\hat{p}_0$ and $\hat{w}_0$ to give

$$\mathscr{L}\hat{u}_0 = \mu\hat{v}_0/\hat{a}^2, \quad \mathscr{L}(\partial_\zeta^2 - 1)\hat{v}_0 = \hat{\theta}_0/\hat{a}^2, \quad \mathscr{N}\hat{\theta}_0 = -(Pr\omega/\hat{a}^2)\hat{v}_0 \qquad (7.12a\text{–}c)$$

$$\hat{u}_0 = \hat{v}_0 = \hat{v}_0 = \hat{\theta}_0 = 0, \quad \zeta = 0, \infty. \qquad (7.12d)$$

A point that should be noticed here is that the x momentum equation decouples from the other equations so that the eigenrelation is determined by the sixth-order system associated with $\hat{v}_0, \hat{\theta}_0$. It is also possible to scale μ and ω out of the above eigenvalue problem by redefining $\hat{a}$ and $\hat{\beta}$. In figure 19 we show the most unstable eigenvalues of (7.12) for $Pr = 1$; the results shown were obtained using a fourth-order finite-difference scheme to discretize the differential equations for $\hat{v}_0$ and $\hat{\theta}_0$.

For small values of $\hat{a}$ we see that $\hat{\beta}_0 \sim \hat{a}$ so that we obtain the required match with the large-wavenumber limiting form of the inviscid mode. The growth rate attains a maximum at a finite value of $\hat{a}$ and then passes through zero at a sufficiently large value of $\hat{a}$. In fact this zero of the growth rate corresponds to the right-hand branch of the neutral curve in the Grashof number–wavenumber plane. Actually it is only possible to find solutions of (7.12) with $\hat{\beta}_0 \neq 0$; the case $\hat{\beta}_0 = 0$ corresponds to the case when

$$-\hat{v}_0 = \hat{\theta}/\hat{a}^2, \; -\hat{\theta}_0 = (Pr\omega/\hat{a}^2)\hat{v}_0,$$

so that $\hat{a}^4 = Pr\omega$ which means that the zeroth-order approximation to the right-hand branch of the neutral curve is given by

$$G = a^4/Pr\omega + \ldots. \qquad (7.13)$$

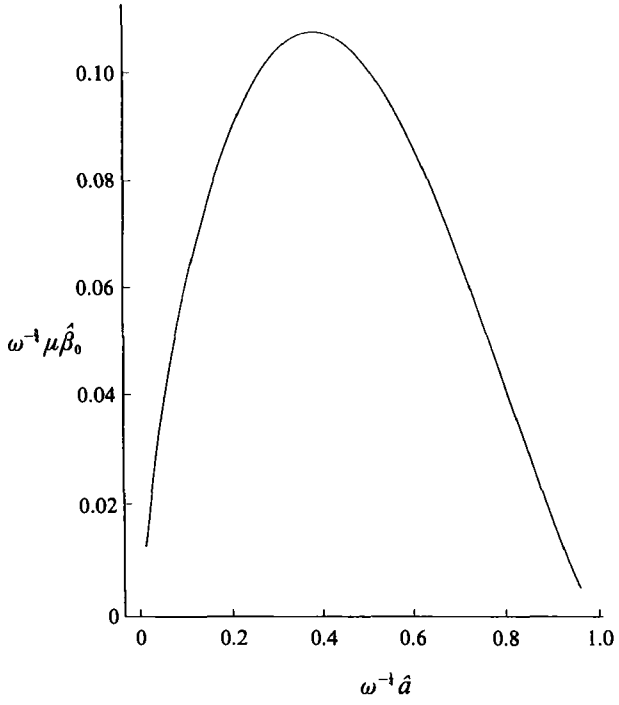

FIGURE 19. The growth rate of the fastest growing viscous mode as a function of wavenumber.

An investigation of (7.12) with $\hat{\beta}_0 \ll 1$ shows that the wall layer becomes thicker in this limit and higher-order terms in (7.13) can be found when it has become $O(G^{-\frac{1}{8}})$; the structure in that case is similar to that found by Hall (1982*a*) for the Taylor problem.

In figure 20 the eigenfunctions $\hat{v}_0, \hat{\theta}_0$ are shown for three different values of the wavenumber. We note that at the largest value of the wavenumber the eigenfunctions have spread further away from the wall whilst at the smallest wavenumber the temperature disturbance develops a wall-layer structure consistent with the inviscid limit discussed above. Thus we have shown above that at high Grashof numbers the fastest growing disturbance is localized at the wall and is dominated by viscous effects. The unstable band of wavenumbers cuts out at the right-hand branch of the neutral curve where $a \sim (Pr\omega G)^{\frac{1}{4}}$. For $a \sim O(1)$ the disturbances are essentially inviscid with a growth rate which leads to zero where $a \to 0$. At some stage viscous effects will reappear for sufficiently small a and then we expect that the left-hand branch of the neutral curve will be encountered. Though the growth rates in this regime are relatively small it is important for disturbances localized very close to the leading edge of the wall since the effective wavenumber of a fixed-wavelength disturbance is small there. In addition there is an unexpected connection between vortex disturbances and Tollmien–Schlichting waves here, so this is now considered in some detail. As a first step we consider the limiting form of (7.3) where $a \to 0$. It is clear from (7.4) that we must consider separately the regions $y = O(1)$ and $y = O(a^{-1})$. For $y = O(1)$ we write

$$u = u_0 + au_1 + \ldots, \quad v = a^{\frac{1}{2}}v_0 + a^{\frac{3}{2}}v_1 + \ldots, \quad w = a^{\frac{1}{2}}w_0 + a^{\frac{3}{2}}w_1 + \ldots, \quad (7.14a\text{–}c)$$

$$\theta = \theta_0 + a\theta_1 + \ldots, \quad p = p_0 + ap_1 + \ldots, \quad (7.14d, e)$$

and $\hat{\beta}_0$ then expands as

$$\hat{\beta}_0 = \hat{\beta}^0 a^{\frac{1}{2}} + \hat{\beta}^1 a + \ldots. \quad (7.15)$$

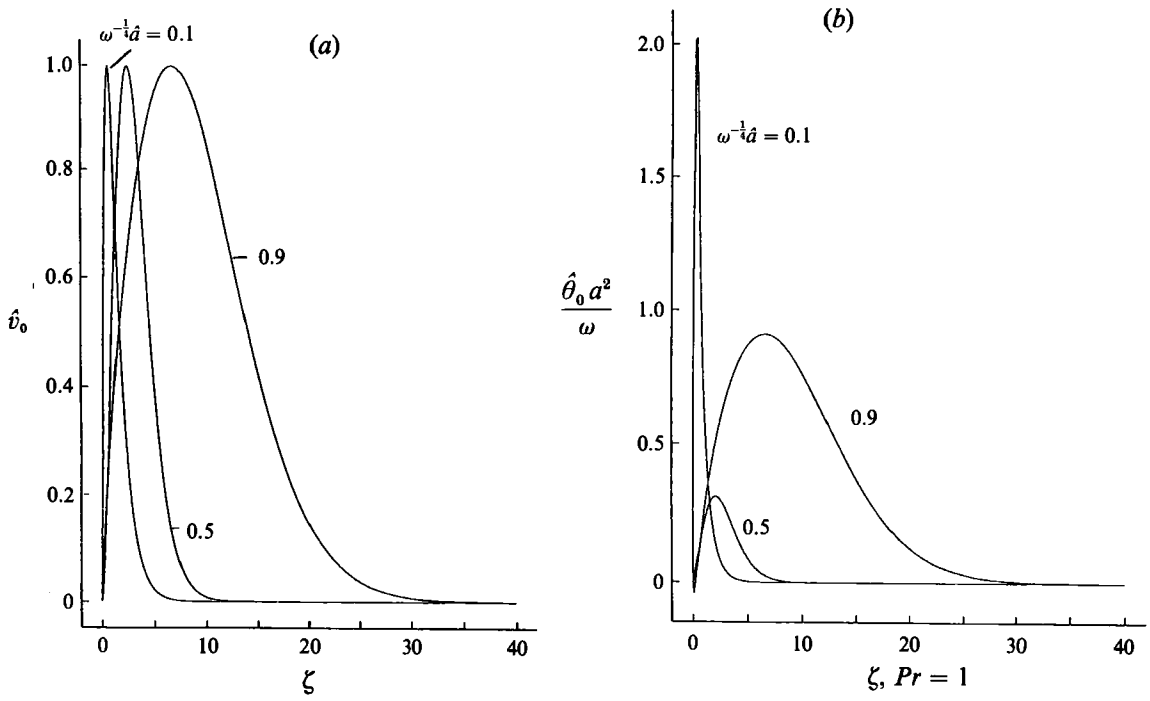

FIGURE 20. The eigenfunctions of (7.12) for different values of the wavenumber, $Pr = 1$. In (*b*) the eigenfunction associated with the smallest wavenumber has been magnified by a factor of 1000.

If we now substitute the above expansions into (7.3) and solve the leading-order approximation to this system we find that

$$u_0 = -\bar{u}_y, \quad v_0 = \hat{\beta}^0\bar{u}, \quad \theta_0 = -\bar{T}_y, \quad p_0 = -\bar{T}+1. \tag{7.16a–d}$$

Meanwhile in the upper, $O(a^{-1})$, layer we can easily show that

$$p = \mathrm{e}^{-ay}+\ldots, \quad v = -(a^{\frac{1}{2}}/\hat{\beta}^0)\,\mathrm{e}^{-ay}+\ldots. \tag{7.17a, b}$$

Thus we can only match the expansions for v in the two layers if

$$(\hat{\beta}^0)^2 = 1$$

so that for small a the eigenrelation associated with (7.3) takes the form

$$\hat{\beta}_0 = a^{\frac{1}{2}}+\ldots. \tag{7.18}$$

The small-a inviscid solution discussed above fails when $\bar{u}\,\partial_x \sim \partial_y^2$ in the layer of depth a^{+1} adjacent to $y = 0$. This occurs when $a \sim G^{-\frac{1}{7}}$ and we then have a triple-deck-like structure with three layers of depth $O(G^{-\frac{1}{7}})$, $O(1)$ and $O(G^{\frac{1}{7}})$ to consider. (Note that the structure described below applies also to the Görtler problem and was alluded to by Denier *et al.* 1991.) We therefore write $a = G^{-\frac{1}{7}}\bar{a}$.

In order to allow for the possibility of unstable Tollmien–Schlichting waves we must modify (2.6) to allow for the possibility of time-dependent modes. This is simply done by inserting the term u_t into the momentum equations and the term θ_t into the temperature equation. In the lower deck where $y = O(G^{-\frac{1}{7}})$ we define $\xi = G^{\frac{1}{7}}y$ and write

$$\{u, G^{-\frac{2}{7}}v, G^{-\frac{4}{7}}w, G^{-1}p, \theta\} = \{(u_0, v_0, w_0, p_0, \theta_0)+\ldots\}\exp\int^x[\hat{\beta}\,\mathrm{d}x - \mathrm{i}\Omega t],$$

where $\hat{\beta} = \hat{\beta}_0 G^{\frac{3}{7}} + \ldots$, $\bar{\Omega} = \Omega G^{\frac{2}{7}} + \ldots$, whilst u_0, v_0, etc. are functions of ξ, x. We assume that the frequency Ω of the disturbance is constant. The equations to determine the zeroth-order approximation to the disturbance in the lower deck are found to be

$$\hat{\beta}_0 u_0 + v_{0\xi} + \mathrm{i}\bar{a} w_0 = 0, \quad -\mathrm{i}\Omega u_0 + \hat{\beta}_0 \mu\xi u_0 + v_0 \mu = u_{0\xi\xi}, \quad 0 = p_{0\xi}, \quad (7.19a\text{–}c)$$

$$-\mathrm{i}\Omega w_0 + \hat{\beta}_0 \mu\xi w_0 = -\mathrm{i}p_0 \bar{a} + w_{0\xi\xi}, \quad -\mathrm{i}\Omega\theta_0 + \hat{\beta}_0 \mu\xi\theta_0 + v_0 \omega = (1/Pr)\,\theta_{0\xi\xi}, \quad (7.19d, e)$$

which must be solved subject to

$$u_0 = v_0 = w_0 = \theta_0 = 0, \quad \xi = 0, \tag{7.20}$$

and appropriate matching conditions at $\xi = \infty$. Thus in the lower deck we have that

$$p = \bar{P}_0, \quad \hat{\beta}_0 u_0 + \mathrm{i}\bar{a} w_0 = \frac{-\bar{a}^2 \bar{P}_0}{\Delta^{\frac{2}{3}} \mathrm{Ai}'(\phi_0)} \int_{\phi_0}^{\phi} \mathrm{Ai}(\tilde{\phi})\,\mathrm{d}\tilde{\phi},$$

where $\bar{P}_0$ is a constant, $\phi = (\mu\hat{\beta}_0)^{\frac{1}{3}}(\xi - \mathrm{i}\Omega/\mu\hat{\beta}_0)$, $\phi_0 = \phi(\xi = 0)$, $\Delta = \hat{\beta}_0 \mu$ and Ai is the Airy function. In the main and upper decks the disturbance takes on essentially the same form as that discussed above for the small-a limit of the inviscid problem. In particular we find that in the main deck

$$p = CG\{(\hat{\beta}_0^2/\bar{a}) - \bar{T}\}, \qquad u = -C\bar{u}_y,$$

where C is a constant.

Thus matching between the main and lower decks is achieved if

$$C\left[\frac{\hat{\beta}_0^2}{\bar{a}} - 1\right] = \bar{P}_0, \quad \hat{\beta}_0 \mu C = \frac{\bar{a}^2 \bar{P}_0}{\Delta^{\frac{2}{3}} \mathrm{Ai}'(\phi_0)} \int_{\phi_0}^{\infty} \mathrm{Ai}\,\mathrm{d}\tilde{\phi},$$

which leads to the eigenrelation

$$\left[-1 + \frac{\hat{\beta}_0^2}{\bar{a}}\right] \bar{a}^2 \int_{\phi_0}^{\infty} \mathrm{Ai}\,\mathrm{d}\tilde{\eta} = \Delta^{\frac{5}{3}} \mathrm{Ai}'(\phi_0). \tag{7.21}$$

We note that if we take the further limit $\bar{a} \to \infty$ we recover the limiting inviscid solution (7.18) whilst in the limit $\bar{a} \to 0$ we obtain

$$-\hat{\beta}_0^2 \bar{a} \int_{\phi_0}^{\infty} \mathrm{Ai}\,\mathrm{d}\tilde{\eta} = \Delta^{\frac{5}{3}} \mathrm{Ai}'(\phi_0), \tag{7.22}$$

and this eigenrelation can be found from the limiting large-wavenumber analysis of Hall & Smith (1984). In fact, rather than solve (7.21) for $\hat{\beta}_0$ as a function of $\bar{a}$, it is more instructive to rewrite this equation using the inverse of the spanwise wavenumber rather than G as the appropriate large parameter. In order to do this we write

$$G = G_0 a^{-7}, \quad \hat{\beta} = \hat{\beta}^* a^{-3}, \quad \Omega = \Omega^* a^{-2}$$

in which case (7.21) becomes

$$-\mathrm{i}^{\frac{1}{3}}\{-G_0 + \hat{\beta}^{*2}\}\chi = \hat{\beta}^{*\frac{5}{3}} \mathrm{Ai}_0', \tag{7.23}$$

where

$$\chi = \int_{-\mathrm{i}^{\frac{1}{3}}\Omega^* \hat{\beta}^{*-\frac{2}{3}}}^{\infty} \mathrm{Ai}(\eta)\,\mathrm{d}\eta, \quad \mathrm{Ai}_0' = \mathrm{Ai}'(-\mathrm{i}^{\frac{1}{3}}\Omega^* \hat{\beta}^{-\frac{2}{3}}). \tag{7.24}$$

If we set $G_0 = 0$ in (7.23) the resulting equation determines the scaled growth rate of a three-dimensional Tollmien–Schlichting wave of frequency Ω^*. By varying G_0 in

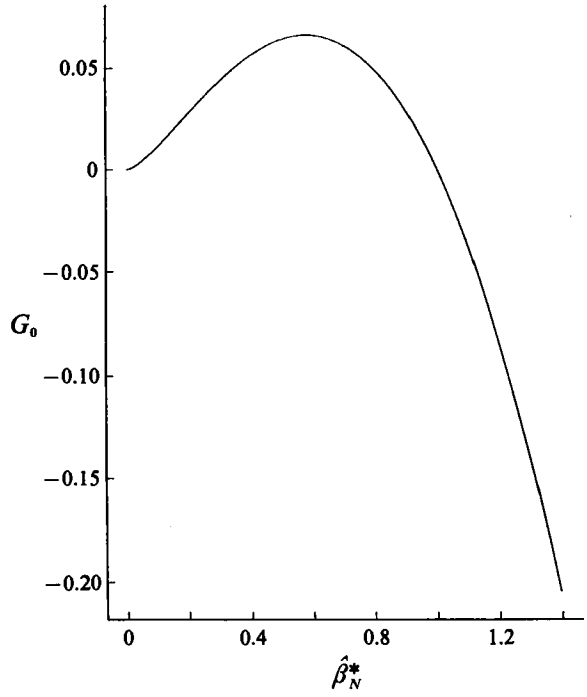

FIGURE 21. The neutral eigenvalues given by (7.26).

the range $-\infty < G_0 < \infty$ we can then infer the effect of heating or cooling on very oblique Tollmien–Schlichting waves. Alternatively, by setting $\Omega^* = 0$ we can obtain the required match with the inviscid low-wavenumber modes discussed earlier. In fact we can see directly from (7.24) that, if $G_0^* \gg 1$ with Ω^* held fixed, then the zeroth-order approximation to the eigenrelation is simply

$$\hat{\beta}_0 = G_0^{\frac{1}{3}} + \ldots, \quad G_0 > 0. \tag{7.25}$$

This corresponds to the limiting inviscid form (7.18) and we also deduce that instability occurs only for positive Grashof numbers. Now we shall present results for the solution of (7.23) for a range of values of G. It is well known that neutral solutions of (7.23) occur when $\mathrm{Ai}_0'/\chi = N\mathrm{i}^{\frac{1}{3}}$ with $N \approx 1.001$. Thus the neutral values of $\hat{\beta}^*$ are given by $\hat{\beta}^* = \mathrm{i}\hat{\beta}_N^*$ where

$$\hat{\beta}_N^{*2} + G_0 = N\hat{\beta}_N^{*\frac{4}{3}}. \tag{7.26}$$

The solutions of this equation are shown in figure 21. The frequency Ω_N associated with each of the neutral points is given by

$$\Omega_N \approx -\mathrm{i}^{\frac{1}{3}} 2.298 \hat{\beta}_N^{\frac{2}{3}}.$$

Thus neutral solutions exist only for non-zero frequencies, although we note that for $G_0 < 0, |G_0| \gg 1$, equation (7.23) yields

$$\hat{\beta}^* = \mathrm{i}|G_0|^{\frac{1}{3}} + \tfrac{1}{2}\mathrm{i}^{\frac{1}{3}}|G_0|^{\frac{1}{3}} A_\infty' \chi^{-1} + \ldots.$$

The leading-order term here reproduces the leading-order neutral inviscid result appropriate to negative Grashof numbers whilst the second viscous term always has negative real part so that the flow is stable in that case. The latter result holds for all frequencies.

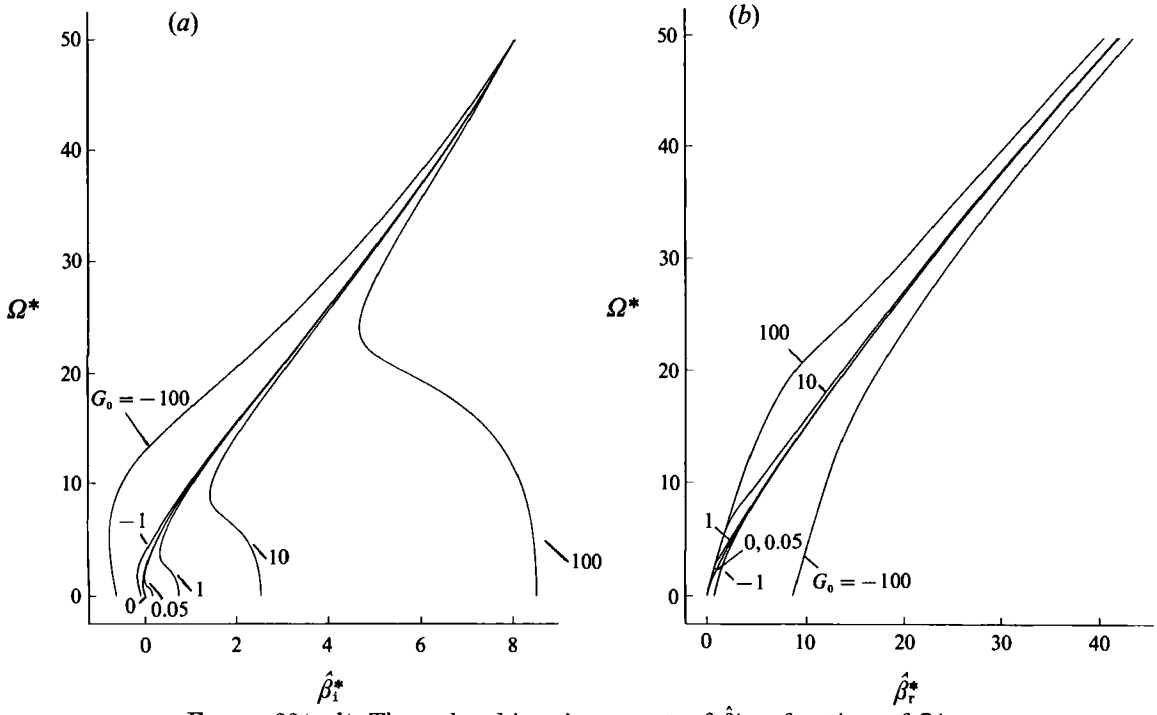

FIGURE 22 (*a*, *b*). The real and imaginary parts of $\hat{\beta}^*$ as functions of Ω^*.

In figure 22 we show the dependence of $\hat{\beta}^*$ on the frequency Ω^* for a range of values of the scaled Grashof number G_0. We see that the mode with $G_0 = 0$ is unstable for $\Omega^* > 2.298, \hat{\beta}^* > 1$. Between $\Omega^* = 0$, 2.298 the mode is stable but we note that the growth rate approaches zero when $\Omega^* \to 0$. If G_0 is now taken to be slightly positive then this limiting neutral point moves to a small positive value of Ω^* and there is then a small but finite band of unstable disturbances of small frequency. When G_0 is increased beyond about 0.06 this unstable band connects with the other unstable band corresponding to the modes with $\Omega^* > 2.298$ for $G = 0$. At this stage there are no neutral solutions and as G_0 is increased the growth rates at small frequencies increase and approach the limiting case $\hat{\beta}^* = |G_0|^{\frac{1}{2}}$ for $G_0 \gg 1$. However, at any fixed value of G_0, we see that the growth rate asymptotes to its Tollmien–Schlichting wave value at sufficiently large values of Ω^*. We conclude that wall heating has a progressively increasing destabilizing effect on Tollmien–Schlichting waves.

If the wall is instead cooled, so that the Grashof number is negative, then the stable band of modes in the interval $0 < \Omega^* < 2.298$ for $G_0 = 0$ increases with the neutral value of $\hat{\beta}_r^*$ given by $\hat{\beta}_r^* |G_0|^{\frac{1}{2}}$ when $G_0 \to -\infty$. However, we again note that for any given value of G_0 the growth rate approaches the Tollmien–Schlichting value at large values of Ω^*.

8. Conclusions

We shall first consider the conclusions to be drawn about the generation of vortex structures by surface imperfections when the spanwise lengthscale is comparable to, but shorter than, the body lengthscale. We have demonstrated how the vortices

develop in a non-parallel manner and shown that a unique growth rate does not exist for a growing vortex structure. We have also shown the neutral curve associated with a particular flow property depends on the upstream history of the disturbance.

In §4 we have discussed the localized forcing problem when the forcing operates on a short streamwise lengthscale. It was shown, for a forcing function of the type considered in §4, that the forcing has the effect of producing a similarity solution of the linear disturbance equations in the region where the forcing is applied. The similarity solution can then be used to form a composite disturbance field associated with an isolated forcing function; if the Grashof number is then varied we can determine the effect of the location of isolated forcing on the onset of instability. Our results show that there is an optimum position for the forcing which will produce instability at the lowest value of the local Grashof number, this lowest value is about 2.

In §5 we have considered the free-stream receptivity problem. We have demonstrated the growth of vortex structures downstream and have shown that the receptivity calculation with $b = 0$ leads to the most dangerous mode. In this case $u_c \sim \cos az$ at the leading edge of the wall. The explanation of this may be that if the disturbance develops in some type of quasi-parallel fashion then for higher values of b the incoming disturbances stimulate the higher modes, which are more stable. It is of interest to note that free-stream disturbances provoke instability at a much lower Grashof number than do roughness induced motions. It would appear then that, in an experiment where care has been taken to reduce the size of disturbances from all sources, it will be the free-stream ones which cause the growth of streamwise vortices.

For the case where the forcing varies on the body lengthscale as discussed in §6 we have demonstrated how the initial disturbance decays and is formed into a wake before its subsequent reamplification within a wedge-shaped region further downstream. We have noted that this type of flow structure has been observed experimentally for the related Görtler-type vortex problem of flow over a concave wall. In fact the results of Gilpin *et al.* (1978) are also consistent with this picture.

The results found in §7 show an unexpected coupling between streamwise vortices and Tollmein–Schlichting waves at low spanwise wavenumbers; in fact in that regime the two types of disturbances are virtually indistinguishable. Though disturbances with much higher growth rates are possible at high Grashof numbers, these low-wavenumber disturbances might be particularly relevant when the forcing mechanism which generates the vortices operates on a long spanwise scale. Moreover it could well be that, even though larger linear growth rates are possible downstream where the local wavenumber has become $O(G_x^{\frac{1}{4}})$, the disturbances might be sufficiently amplified near the left-hand branch of the neutral curve for nonlinear effects to come into play. In that case the fact that larger linear growth rates were available downstream would be irrelevant.

We now make some further comparisons with previous theoretical and experimental results. In order to make such comparisons it is convenient to define the parameters

$$Gr_x = g\hat{\beta}T_0 x^{*3}/\nu^2, \quad Re_x = U_\infty x^*/\mu.$$

The local Grashof number in our notation, G_x, is then given by $G_x = Gr_x Re_x^{-\frac{3}{4}}$. Thus if the instability is caused by wall forcing we expect that instability will occur whenever $Gr_x Re_x^{-\frac{3}{4}} > \sim 2$. Wu & Cheng (1976) made a parallel-flow stability analysis of the problem investigated here and found that for air instability occurred for $Gr_x Re_x^{-\frac{3}{4}} \gtrsim 292$. Later results given by Moutsoglou *et al.* (1981) contradicted those of Wu & Cheng and figure 1 of their paper suggest instability at zero Grashof number.

This result is not unlike some of the physically unrealistic results given by parallel-flow theories of Görtler vortex growth. In order to remove this difficulty Moutsoglou *et al.* retained higher-order buoyancy effects even though they are formally negligible. The latter approach is equivalent to the attempts made to alleviate the corresponding Görtler problem by retaining higher-order curvature effects. Our results show that if non-parallel effects are accounted for in a self-consistent matter then instability occurs at a finite Grashof number and the difficulty is not present.

Wang (1982) investigated experimentally the onset of the vortex instability; his results suggest that instability occurs for $Gr_x Re_x^{-\frac{5}{3}} \gtrsim 55$. This is not consistent with our prediction which has the $\frac{5}{3}$ power replaced by $\frac{3}{2}$. We presume that the experimental result is not consistent with ours because of the uncertainty associated with identifying the onset of vortex activity.

This research was supported in part by the National Aeronautics and Space Administration under NASA Contract No. NAS1-18605 while the author was in residence at the Institute for Computer Applications in Science and Engineering (ICASE), NASA Langley Research Center, Hampton, VA 23665. This work was also supported by SERC. The authors wish to acknowledge the help of Dr J. Gajjar in connection with the numerical work of this paper.

REFERENCES

Akiyama, M., Hwang, G. J. & Cheng, K. C. 1971 Experiments on the onset of longitudinal vortices in laminar forced convection between horizontal plates. *Trans. ASME* C: *J. Heat Transfer* **93**, 335–341.

Chen, K. & Cheng, M. M. 1984 Thermal instability of forced convection boundary layers. *Trans. ASME* C: *J. Heat Transfer* **106**, 284–289.

Denier, J. P., Hall, P. & Seddougui, S. 1991 On the receptivity problem for Görtler vortices: vortex motion induced by wall roughness. *Phil. Trans. R. Soc. Lond.* A **334**, 51–85.

Gilpin, R. R., Imura, H. & Cheng, K. C. 1978 Experiments on the onset of longitudinal vortices in horizontal Blasius flow heated from below. *Trans. ASME* C: *J. Heat Transfer* **100**, 71–77.

Hall, P. 1982*a* Taylor-Görtler vortices in fully developed or boundary layer flows: linear theory. *J. Fluid Mech.* **124**, 475–494.

Hall, P. 1982*b* On the nonlinear evolution of Görtler vortices in nonparallel boundary layers. *J. Inst. Maths Applics.* **29**, 173–196.

Hall, P. 1983 The linear development of Görtler vortices in growing boundary layers. *J. Fluid Mech.* **130**, 41–58.

Hall, P. 1990 Görtler vortices in growing boundary layers: the leading edge receptivity problem, linear growth and the nonlinear breakdown stage. *Mathematika* **37**, 151–189.

Hall, P. & Smith, F. T. 1984 On the effects of nonparallelism, three-dimensionality and mode interaction in boundary layer stability theory. *Stud. Appl. Maths* **70**, 91–120.

Mangalam, S. M., Dagenhart, J. R. & Meyers, J. F. 1991 Experimental studies on Görtler vortices. *NASA Symp. on Natural Laminar Flow and Laminar Flow Control Research. NASA TM* (in press).

Moutsoglou, A., Chen, T. S. & Cheng, K. C. 1981 Vortex Instability of mixed convection flow over a Horizontal Flat Plate. *Trans. ASME* C: *J. Heat Transfer* **103**, 257–261.

Wang, X. A. 1982 An experimental study of mixed, forced and free convection heat transfer from a horizontal plate to air. *Trans. ASME* C: *J. Heat Transfer* **104**, 139–144.

Wu, R. S. & Cheng, K. C. 1976 Thermal instability of Blasius flow along horizontal plates. *Intl J. Heat Mass Transfer* **105**, 907–913.